



## Research papers

## Uncertainties in partitioning evapotranspiration by two remote sensing-based models

Huiling Chen<sup>a</sup>, Gaofeng Zhu<sup>a,\*</sup>, Shasha Shang<sup>a</sup>, Wenhua Qin<sup>a</sup>, Yang Zhang<sup>a</sup>, Yonghong Su<sup>b</sup>, Kun Zhang<sup>c,d</sup>, Yongtai Zhu<sup>a</sup>, Cong Xu<sup>a</sup>

<sup>a</sup> College of Earth and Environmental Sciences, Lanzhou University, Lanzhou 730000, China

<sup>b</sup> Northwest Institute of Eco-Environment and Resources, Chinese Academy of Sciences, Lanzhou, China

<sup>c</sup> School of Biological Sciences, The University of Hong Kong, Hong Kong, China

<sup>d</sup> Department of Mathematics, The University of Hong Kong, Hong Kong, China

## ARTICLE INFO

## Keywords:

Evapotranspiration  
Partitioning  
Interception  
Soil evaporation  
Transpiration

## ABSTRACT

Accurate estimation of evapotranspiration (ET) and the partitioning of ET into transpiration ( $T_r$ ), soil evaporation ( $E_s$ ) and interception ( $E_i$ ) is critical to understand water cycle and land-atmosphere feedback. In this study, we evaluated the performances of two remote sensing-based ET models at multiple scales, and analyzed the uncertainties in ET partitioning due to the model structures. These two models were Simple Terrestrial Hydrosphere Model (SiTH) developed by our team and the Global Land Evaporation Amsterdam Model (GLEAM). As far as ET were concerned, the two models exhibited relatively good performances at different scales. However, it was found that GLEAM performed relatively poor at evergreen broadleaf forest ( $R^2 = 0.34$ ; RMSE = 0.87 mm day $^{-1}$ ; NSE = -0.28). In addition, the seasonal pattern of simulated ET by GLEAM at the tropical rainforest was not consistent with the observations. Furthermore, great discrepancies in ET partitioning were observed between the two models. Generally, GLEAM tended to underestimate  $E_s$  (slope = 0.02;  $R^2 = 0.004$ ), and overestimate  $T_r$  (slope = 1.51;  $R^2 = 0.78$ ) compared to the observations. The underestimations of  $E_s$  by GLEAM may partly be due to the ignorance of soil evaporation under vegetation canopy. On the contrary, SiTH displayed relatively good performances in estimations of  $E_s$  (slope = 0.76;  $R^2 = 0.62$ ) and  $T_r$  (slope = 0.98;  $R^2 = 0.51$ ). However, both of the two models failed to properly simulate  $E_i$ , although GLEAM (slope = 0.55;  $R^2 = 0.83$ ) performed slightly better than SiTH (slope = 0.40;  $R^2 = 0.95$ ). Global multi-year average ratios of  $T_r$ ,  $E_s$ , and  $E_i$  to ET for GLEAM and SiTH were 0.76, 0.09, 0.15 and 0.67, 0.25, 0.08 respectively. In future studies, it is important to investigate direct observations on different components of ET, especially on the interception, to improve our understanding on the ET processes.

## 1. Introduction

As a key part of global water cycle, evapotranspiration (ET) is a critical nexus between terrestrial water, carbon and surface energy exchanges (Oki and Kanae, 2006; Trenberth et al., 2009; Vinukollu et al., 2011a; Wang and Dickinson, 2012; Kool et al., 2014). In general, ET is mainly consisted of three components: plant transpiration ( $T_r$ ), soil evaporation ( $E_s$ ), and canopy interception ( $E_i$ ). Among them,  $T_r$  is a biotic process regulated by plant stomatal activities (Granier et al., 1999; Kool et al., 2014; Kumar et al., 2018; Han et al., 2018), while  $E_i$  and  $E_s$  are physical processes that directly convert the water from liquid to vapour by energy (Scott et al., 2006; Kool et al., 2014; Wang et al.,

2014). Therefore, accurate estimations of the total ET and its components are important for us to understand the land-atmosphere interactions, water and energy balances, and agricultural water demands (Newman et al., 2006; Lawrence et al., 2007; Wang and Dickinson, 2012; Kool et al., 2014; Talsma et al., 2018).

At present, the ET and its components can be measured in situ by using different techniques, such as eddy covariance systems, stable isotope, sap flow, and micro-lysimeters (Talsma et al., 2018; Berg and Sheffield, 2019). However, large-scale direct observations of the ET components are still not available. With the rapid developments in remote sensing over the recent four decades, numerous ET models have been developed to estimate regional or global ET and its different

\* Corresponding author.

E-mail address: zhugf@lzu.edu.cn (G. Zhu).

components (Norman et al., 1995; Cleugh et al., 2007; Mu et al., 2007, 2011; Leuning et al., 2008; Zhang et al., 2010; Fisher et al., 2008; Miralles et al., 2011; Zhang et al., 2016; Zhu et al., 2019). However, many of the remote sensing-based models lack a proper representation of the effects of soil moisture status on ET, and the performance of those models suffers when applied to water-limited areas (Purdy et al., 2018; Chen et al., 2020). For example, the Priestley-Taylor Jet Propulsion Laboratory (PT-JPL; Fisher et al., 2008) model and the MODIS Global Evapotranspiration Project (MOD16; Mu et al., 2011) model use the atmospheric moisture conditions (i.e. air temperature, relative humidity and vapour pressure deficit) to represent the soil moisture constraints on ET. Exceptionally, the Global Land Evaporation Amsterdam Model (GLEAM; Miralles et al., 2011) and Simple Terrestrial Hydrosphere Model (SiTH; Zhu et al., 2019) directly describe the soil moisture dynamics with reliance on the water balance equations, and explicitly represent the control of soil water availability on ET processes. Thus, they are physically sound and rigorous, and performed relatively good across different ecosystem types and environments (Purdy et al., 2018; Brust et al., 2021).

Despite their relatively sound representations of associated hydrological processes, there are still some insufficiencies in systematic inter-comparisons and evaluations of their performances. First, the partitioning of ET into its different components exhibited large divergences among the different models (Wang-Erlandsson et al., 2014; Miralles et al., 2016; Talsma et al., 2018; Berg and Sheffield, 2019). At present, most previous studies mainly focus on evaluating the performance of the models in simulating the total ET (Vinukollu et al., 2011b; Ershadi et al., 2014; Miralles et al., 2016), while researches on systematically comparing the performance of the different models in ET partitioning across different biomes are still few or no-existed. Second, the remote sensing-based models use different bio-physiological stress functions to tune down the potential ET to actual ET (Fisher et al., 2008; Mu et al., 2007; Miralles et al., 2011; Zhu et al., 2019). Hence, their performance in partitioning ET are expected to differ over various land surface types and conditions. However, there are lack of systematic assessments on the uncertainties in ET partitioning due to the model structures. Therefore, a basis from which to choose a proper parameterization for the different ET processes remains missing. Finally, there are still great uncertainties in ET partitioning across different sites and biomes, and the seasonal variability of the model performances remains unclear.

To further improve the estimations of ET and its components, we compared and analyzed these two model's performances over a wide range of locations and biomes. Specifically, the goals of this study were to (i) evaluate the performance of the models in simulating total ET and its components with the field observations, (ii) analyze the spatial pattern similarities and differences of estimated ET and its components by these two models, and (iii) find out the uncertainties in total ET and its components due to model structure.

## 2. Methods and data

### 2.1. ET models

In GLEAM and SiTH models, the potential ET is calculated using the Priestley-Taylor (PT) equation (Priestley and Taylor, 1972), then is tuned down to actual ET based on the stress factors such as soil moisture states and vegetation physiological characteristics. The details of the two models were given below.

#### 2.1.1. GLEAM model

GLEAM is a simple and widely used remote sensing-based ET model. The total ET ( $\text{mm day}^{-1}$ ) mainly includes the transpiration ( $T_v$ ,  $\text{mm day}^{-1}$ ) from short (e.g. grass) and tall canopy vegetation (e.g. trees), soil evaporation ( $E_s$ ,  $\text{mm day}^{-1}$ ) from bare soil and interception ( $E_i$ ,  $\text{mm day}^{-1}$ ) from tall vegetation (Miralles et al., 2011). In GLEAM, each grid contains three land covers of short vegetation, tall vegetation, and bare

soil. The total ET of the grid is the sum of the actual evaporation from each of the three surface types weighted by their fractional coverage. The interception is calculated separately using the Gash model (Gash, 1979; Valente et al., 1997).  $E_s$  and  $T_r$  are calculated using a series of stress factors to constrain the PT potential evapotranspiration, expressing as the following equations:

$$E_s = r_s S_s \alpha_s \frac{\Delta}{\lambda(\Delta + \gamma)} (R_n^s - G_s) \quad (1)$$

$$T_r = r_{sc} S_{sc} \alpha_{sc} \frac{\Delta}{\lambda(\Delta + \gamma)} (R_n^{sc} - G_{sc}) + r_{tc} S_{tc} \alpha_{tc} \frac{\Delta}{\lambda(\Delta + \gamma)} (R_n^{tc} - G_{tc}) - \beta E_i \quad (2)$$

where the  $\Delta$  is the slope of the saturated vapour pressure curve ( $\text{kPa } ^\circ\text{C}^{-1}$ );  $\lambda$  is the latent heat of vaporization ( $\text{MJ kg}^{-1}$ ), and represents the energy required to change a unit mass of water from liquid to water vapour in a constant pressure and temperature process;  $\gamma$  is the psychrometric constant ( $0.066 \text{ kPa } ^\circ\text{C}^{-1}$ ), which is the ratio of specific heat of moist air at constant pressure to latent heat of vaporization of water;  $r_s$ ,  $r_{sc}$  and  $r_{tc}$  are the fractions of bare soil, short vegetation, and tall vegetation in each pixel, respectively;  $\alpha$  is the PT coefficient (Priestley and Taylor, 1972) and is set respectively to 1.26, 1.26 and 0.80 for bare soil ( $\alpha_s$ ), short vegetation ( $\alpha_{sc}$ ) and tall vegetation ( $\alpha_{tc}$ ) in GLEAM;  $R_n^s$ ,  $R_n^{sc}$  and  $R_n^{tc}$  ( $\text{W m}^{-2}$ ) are the net radiation intercepted by bare soil, short vegetation and tall vegetation, respectively;  $G_s$ ,  $G_{sc}$ , and  $G_{tc}$  ( $\text{W m}^{-2}$ ) are the soil heat flux for the fraction of bare soil, short vegetation, and tall vegetation, respectively, being as fractions of net radiation in GLEAM; and  $\beta$  is the interception constant (0.07), which is used to avoid the double counting of evaporation from wet canopy (Gash and Stewart, 1977).

In GLEAM, the stress factors are parameterized separately for tall canopies ( $S_{tc}$ ), short vegetation ( $S_{sc}$ ), and bare soil ( $S_s$ ), which are the function of the soil moisture and the vegetation water content (i.e. vegetation optical depth (unitless), VOD). The stress factors for the tall vegetation and short vegetation are calculated as:

$$S_{tc} \text{ or } S_{sc} = \sqrt{\frac{VOD}{VOD_{max}}} \left( 1 - \left( \frac{\theta_c - \theta^{(w)}}{\theta_c - \theta_{wp}} \right)^2 \right) \quad (3)$$

where  $VOD_{max}$  is the maximum VOD for a specific pixel;  $\theta_c$  ( $\text{m}^3 \text{ m}^{-3}$ ) is the critical soil moisture below which plants start to endure water stress;  $\theta^{(w)}$  ( $\text{m}^3 \text{ m}^{-3}$ ) is the soil moisture content of the wettest layer; and  $\theta_{wp}$  is soil moisture at permanent wilting point ( $\text{m}^3 \text{ m}^{-3}$ ). In addition, the stress factor for bare soil ( $S_s$ ) is calculated based on surface soil water states:

$$S_s = 1 - \frac{\theta_c - \theta^{(1)}}{\theta_c - \theta_r} \quad (4)$$

where  $\theta_r$  is the residual soil moisture ( $\text{m}^3 \text{ m}^{-3}$ ); and  $\theta^{(1)}$  is the surface soil moisture ( $\text{m}^3 \text{ m}^{-3}$ ).

#### 2.1.2. SiTH model

Following the scheme of the groundwater-soil-plant-atmosphere continuum, SiTH model proposed by Zhu et al. (2019) is a relatively new satellite-based ET model at daily temporal resolution. In SiTH model, the total ET is the sum of vegetation transpiration, soil evaporation and canopy interception evaporation. The source of water for soil evaporation is constrained to occur in the first soil layer, while its for plant transpiration comes from both two soil layers and groundwater. For the interception loss, rainfalls intercepted by the canopy are evaporated at the potential rate. These can be described as:

$$E_i = f_{WET} \times \alpha \frac{\Delta}{\Delta + \gamma} \frac{R_{nc}}{\lambda} \quad (5)$$

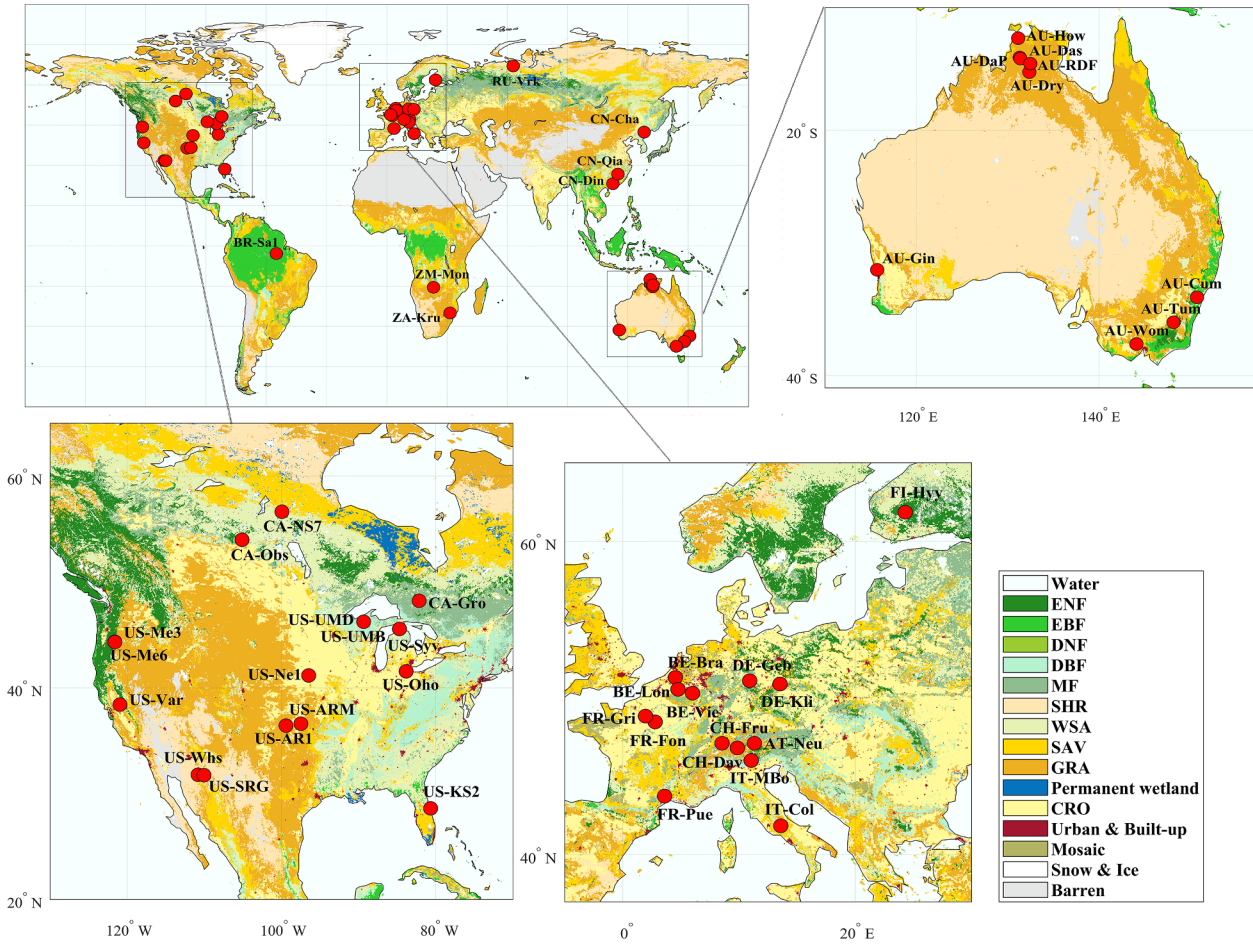


**Fig. 1.** Flux sites used in the study. Land cover is derived from the MODIS-based MCD12C1 product.

$$E_s = f_{SM} \times \alpha \frac{\Delta}{\Delta + \gamma} \frac{(R_{ns} - G)}{\lambda} \quad (6)$$

$$T_{r,g} = (1 - f_{WET}) \times f_T \times \sum_{i=1}^n T_{p-g,i} \quad (7)$$

$$T_{s,i} = (1 - f_{WET}) \times f_{SM,i} \times f_T \times T_{p-s,i} \quad (8)$$

$$T_r = T_{s,i} + T_{r,g} \quad (9)$$

where  $i$  is the soil layer ( $i = 1, 2$ ); The  $\alpha$  is set to 1.26 in SiTH;  $R_{nc}$  and  $R_{ns}$  ( $\text{W m}^{-2}$ ) are the net radiation distributed into the canopy and surface soil, respectively;  $T_{p,s,i}$  and  $T_{p,g,i}$  ( $\text{mm day}^{-1}$ ) are respectively the potential transpiration from soil water and groundwater in the  $i$ th layer, which are calculated using the PT potential ET by taking the vertical distributions of plant roots and the position of groundwater table into accounts (see details in Zhu et al., 2019);  $T_{s,i}$  and  $T_{r,g}$  ( $\text{mm day}^{-1}$ ) are the actual transpiration from the soil of the  $i$ th layer and groundwater, respectively;  $f_{WET}$  is the relative surface wetness (unitless), which is fraction of day-time consumed by wet canopy evaporation;  $f_T$  is the plant temperature constraint (unitless);  $f_{SM,i}$  is the soil moisture constraint (unitless) of the  $i$ th soil layer. These constraint functions are calculated as below:

$$f_{WET} = \min\left\{\chi \frac{S_c}{T_p}, 1\right\} \quad (10)$$

$$f_T = \exp\left[-\left(\frac{T_a - T_{opt}}{T_{opt}}\right)^2\right] \quad (11)$$

$$f_{SM,i} = \begin{cases} 0 & \theta_i \leq \theta_{wp,i} \\ 1 - \left(\frac{\theta_{ci} - \theta_i}{\theta_{ci} - \theta_{wp,i}}\right)^2 & \theta_{wp,i} < \theta_i < \theta_{ci} \\ 1 & \theta_i \geq \theta_{ci} \end{cases} \quad (12)$$

where  $\chi$  is fractional interception occurring during day-time (0.7);  $S_c$  ( $\text{mm day}^{-1}$ ) is the capacity of canopy to store water, defined as a function of biome, incoming rainfall, and leaf area index;  $T_a$  ( $^\circ\text{C}$ ) is the air temperature;  $T_{opt}$  ( $^\circ\text{C}$ ) is the optimum temperature for canopy transpiration, which is the air temperature value when the multiply of leaf area index, net radiation and air temperature reaches the maximum in a year;  $\theta_{ci}$  ( $\text{m}^3 \text{m}^{-3}$ ) is the critical soil moisture for soil layer  $i$ ; and  $\theta_{wp,i}$  ( $\text{m}^3 \text{m}^{-3}$ ) is soil moisture at permanent wilting point for the  $i$ th soil layer.

## 2.2. Analysis methods

Five statistical measures are used to represent the model performance, including the slope of the regression line (slope), the coefficient of determination ( $R^2$ ), root-mean-square error (RMSE), the relative error (RE) and the Nash-Sutcliffe efficiency coefficient (NSE). Generally, the  $R^2$  value of linear regression between simulations and observations greater than 0.5 is considered as acceptable performance. The RMSE shows the magnitude and variance in error between observed and simulated values, ranging from 0 to  $+\infty$ . The RE is defined as the ratio of RMSE to the mean values of observed data. The NSE is a normalized statistic that determines the relative magnitude of the residual variance compared to the measured data variance. When the NSE values is closer to 1, the simulation is better. The RMSE, RE and NSE were computed as:

**Table 1**The information of 46 flux sites used for model validation. More details can be found at <https://fluxnet.fluxdata.org>.

No.	Site	Lat.	Lon.	year_start	year_end	Elevation (m)	MAP (mm year <sup>-1</sup> )	MAT (°C)	Reference
<i>ENF</i>									
1	US-Me3	44.31	-121.61	2004	2009	1005	719	7.07	Vickers et al. (2009)
2	US-Me6	44.32	-121.61	2010	2014	998	494	7.59	Ruehr et al. (2012)
3	CA-Obs	53.99	-105.12	1997	2010	628.94	405.60	0.79	Brooks et al. (1997)
4	FI-Hyy	61.85	24.29	2000	2014	181	709	3.80	Suni et al. (2003)
5	CH-Dav	46.82	9.86	1997	2014	1639	1062	2.80	Zielis et al. (2014)
<i>EBF</i>									
6	AU-Cum	-33.62	150.72	2012	2014	-	-	-	Beringer et al. (2016)
7	AU-Tum	-35.66	148.15	2001	2014	1200	1159.01	10.72	Leuning et al. (2005)
8	CN-Din	23.17	112.54	2003	2005	-	1618.10	19.64	Yu et al. (2006)
9	FR-Pue	43.74	3.60	2000	2014	270	883	13.50	Rambal et al. (2004)
10	AU-Wom	-37.42	144.09	2010	2014	705	-	-	Beringer et al. (2016)
11	BR-Sa1	-2.86	-54.96	2002	2004	88	2548.17	26.13	Saleska et al. (2003)
<i>DBF</i>									
12	FR-Fon	48.48	2.78	2005	2014	103	720	10.20	Delpierre et al. (2016)
13	IT-Col	41.85	13.59	1996	2014	1560	1180	6.30	Valentini et al. (1996)
14	US-Oho	41.55	-83.84	2004	2013	230	849	10.10	Noormets et al. (2008)
15	US-UMB	45.56	-84.71	2000	2014	234	803	5.83	Rothstein et al. (2000)
16	US-UMd	45.56	-84.70	2007	2014	239	803	5.83	Hardiman et al. (2011)
17	ZM-Mon	-15.44	23.25	2000	2009	1053	945	25.00	Merbold et al. (2009)
18	CN-Qia	26.74	115.06	2003	2005	-	1466.75	18.95	Yu et al. (2006)
<i>MF</i>									
19	BE-Bra	51.31	4.52	1996	2014	16	750	9.80	Carrara et al. (2004)
20	BE-Vie	50.30	6.00	1996	2014	493	1062	7.80	Aubinet et al. (2001)
21	CA-Gro	48.22	-82.16	2003	2014	340	831	1.30	McCaughey et al. (2006)
22	CN-Cha	42.40	128.10	2003	2005	-	663.59	2.16	Guan et al. (2006)
23	US-Syv	46.24	-89.35	2001	2014	540	826	3.81	Desai et al. (2005)
<i>GRA</i>									
24	US-AR1	36.43	-99.42	2009	2012	611	-	-	Baldocchi and Penuelas (2018)
25	US-SRG	31.79	-110.83	2008	2014	1291	420	17.00	Scott et al. (2015)
26	AT-Neu	47.12	11.32	2002	2012	970	852	6.50	Wohlfahrt et al. (2008)
27	AU-DaP	-14.06	131.32	2007	2013	-	983.78	27.25	Beringer et al. (2011)
28	IT-MBo	46.01	11.05	2003	2013	1550	1214	5.10	Marcolla et al. (2011)
29	CH-Fru	47.12	8.54	2005	2014	982	1651	7.20	Imer et al. (2013)
30	US-Var	38.41	-120.95	2000	2014	129	559	15.8	Ma et al. (2007)
<i>CRO</i>									
31	BE-Lon	50.55	4.75	2004	2014	167	800	10.00	Moureaux et al. (2006)
32	DE-Geb	51.10	10.91	2001	2014	161.51	470	8.50	Anthoni et al. (2004)
33	DE-Kli	50.89	13.52	2004	2014	478	842	7.60	Prescher et al. (2010)
34	FR-Gri	48.84	1.95	2004	2014	125	650	12.00	Loubet et al. (2011)
35	US-ARM	36.61	-97.49	2003	2012	314	843	14.76	Raz-Yaseef et al. (2015)
36	US-Ne1	41.17	-96.48	2001	2013	361	790.37	10.07	Suyker et al. (2004)
<i>SAV</i>									
37	AU-Das	-14.16	131.39	2008	2014	-	975.82	27.22	Hutley et al. (2011)
38	AU-Dry	-15.26	132.37	2008	2014	-	-	-	Cermusak et al. (2011)
39	ZA-Kru	-25.02	31.50	2000	2013	359	547	21.90	Archibald et al. (2009)
<i>WSA</i>									
40	AU-Gin	-31.38	115.71	2011	2014	-	-	-	Beringer et al. (2016)
41	AU-How	-12.49	131.15	2001	2014	-	1449.35	27.01	Beringer et al. (2007)
42	AU-RDF	-14.56	132.48	2011	2013	-	-	-	Bristow et al. (2016)
<i>SHR</i>									
43	CA-NS7	56.64	-99.95	2002	2005	297	483.27	-3.52	Wang et al. (2003)
44	US-Whs	31.74	-110.05	2007	2014	1370	320	17.60	Scott et al. (2015)
45	US-KS2	28.61	-80.67	2003	2006	3	1294	21.66	Hymus et al. (2003)
46	RU-Vrk	67.05	62.94	2008	2008	100	501	-5.60	Thomas et al. (2016)

\*MAP is the mean annual precipitation (mm year<sup>-1</sup>); MAT is the mean annual temperature (°C).

$$RMSE = \sqrt{\frac{1}{n} \sum_{t=1}^n [O(t) - S(t)]^2} \quad (13)$$

$$RE = \frac{RMSE}{\bar{O}} \quad (14)$$

$$NSE = 1 - \frac{\sum_{t=1}^n [O(t) - S(t)]^2}{\sum_{t=1}^n [O(t) - \bar{O}]^2} \quad (15)$$

where  $n$  is the total number of observations;  $O(t)$  is the observed ET at time  $t$ ,  $S(t)$  is the simulated ET, and  $\bar{O}$  is the mean of observed values.

### 2.3. Data

#### 2.3.1. Model forcing data

The inputs variables of the SiTH include leaf area index (LAI), net radiation (Rn), air temperature (Ta), precipitation (PRE), air pressure (Pa), and land cover (LC). Here, we used input datasets for LAI from GLOBMAP LAI for 1982 to 2017 (Liu et al., 2012). The GLOBMAP LAI is generated in 8 km and 16-day/8-day resolution, produced by using

**Table 2**

List of field studies used to validate ET partitioning. Locations, characteristics, observational method and duration in situ observations of ET and its components are compiled from the literature.

Lat.	Lon.	PFT	MAP	MAT	Method	Period of Measurements	ET	$T_r$	$E_s$	$E_i$	Reference
-4.69	12.08	EBF	1188	24.9	$I_{obs}$	1996.11.1–1997.4.30				47	Nizinski et al. (2011)
						1997.11.1–1998.4.30				140.50	
						1998.11.1–1999.4.30				148.90	
23.17 9.58	112.50 -83.73	EBF	1678	20.9	EC, sap flow $I_{obs}$	2010.7–2011.6	836.60	503.30			Liu et al. (2015)
						1999.9–2000.8				611	Hölscher et al. (2004)
-2.95	-57.95	EBF			EC	1983.9–12	425				Shuttleworth (1988)
						1984.1–12		1393			
						1985.1–9			930		
45.82	-121.95	ENF			$I_{obs}$	1999.4.8–11.8				102.70	Link et al. (2004)
						2000.3.30–12.3				155	
-43.20	170.30	ENF	3400	11.30	EC, sap flow	2001.11–2002.3		83.60			Barbour et al. (2005)
46.23	-89.33	DBF	896	3.80	EC, sap flow	2002(160–261)			161.16		Tang et al. (2006)
						2003(152–264)			176.28		
38.66	-120.63	Forest	1270	9.20	EC, sap flow	growing season mean	261				Kurpius et al. (2003)
						2000(153–359)		496.58	266.81		Granier et al. (2000)
						1996.5.2–10.27	338				Stoy et al. (2006)
						1997.5.2–10.27	357		256		
						2001	261				
						2001.4–9	610				
						2002	490				
						2002.4–9	580				
						2003	480				
						2003.4–9	640				
36.12	140.10	Forest	1207	14.10	Sap flow	2004	510				
						2004.4–9	640				
31.30	35.03	Forest	285		EC, sap flow, micro-lysimeters	2004.9–1985.8	500				Iida et al. (2006)
						2001.8–2002.7	344				
						2003.10–2004.9	420				
						2004.10–2005.9	235	134	99		Raz-Yaseef et al. (2012)
						2005.10–2006.9	343	156	112		
50.03	6	Forest		15.50	EC	2006.10–2007.9	227	111	93		
						2006.10–2007.9	263	115	106		
						2010(171–274)				46	Soubie et al. (2016)
						2011(120–279)				49	
						2010(184–266)	149.40				
60.30 35.95	17.29 -84.28	MF	527	5.50	EC, sap flow, $I_{obs}$ EC, Soil water budget	2011(166–277)	190.40				
						2010(141–275); 2011(127–281)	377				
						1995.5.16–10.31	339	243		74	Grelle et al. (1997)
						1998	547		86		Wilson et al. (2001)
						1998	605		91		
31.91	-110.84	OSH	345	20	Sap flow	2008(200–285)		54.70	31.91		Cavanaugh et al. (2011)
31.74	-110.05	OSH	340	17	Sap flow	2008(205–274)		44.50	31.74		Cavanaugh et al. (2011)
31.7 36.92 40.67	-110.10 -116.55 -104.75	OSH	322	15.60	Stable isotopes	Sap flow	121				Scott et al. (2006)
						LI-1600	40				Smith et al. (1995)
						2000.5–10	210.45				Ferretti et al. (2003)
42.97	122.35	GRA	474		EC, $I_{obs}$	2001.5–10	272				
						2011.5–9	260.50				Song et al. (2018)
34.33	108.07	CRO	521	12.90	Sap flow, micro-lysimeters	2012.5–9	372.70				Ma et al. (2020)
						2014.10.18–2015.8.18	258.10	82.90			
34.30	108.40	CRO	560	12.90	Sap flow, Micro-lysimeters	2015.10.09–2016.8.25	217.20	88.60			
						2015.6.15–2015.9.30	155.49	74.90			Zheng et al. (2021)
39.62	116.43	CRO	540	12.10	Stable isotopes	2016.6.12–2016.10.4	126.28	81.11			
						2017.6.14–2017.10.6	168.29	81.86			
35.27	107.67	CRO	584		sap flow, Micro-lysimeters	2013.10.9–2014.6.8	270.10	224.40			Ma and Song (2019)
						2014.10.11–2015.6.8	315.40	252.70			
-32.32	117.87	CRO	361		EC	2012.5–9	131.50	177.50			Wang and Wang (2017)
						2013.5–9	135	176.70			
21.08 20.90 -28.55	109.90 109.87 -66.82	CRO			EC, sap flow, $I_{obs}$ , Micro-lysimeters	2014.5–9	124	167.40			Mitchell et al. (2009)
						2006.8	7.13	24.90			Zhou et al. (2004)
21.08 20.90 -28.55	109.90 109.87 -66.82	CRO			Sap flow, Micro-lysimeters	2006.11	60	18.91			Rousseaux et al. (2009)

\* The EC is the eddy covariance systems. The  $I_{obs}$  represents that interception is measured by the difference between gross rainfall and the sum of throughfall and stemflow.

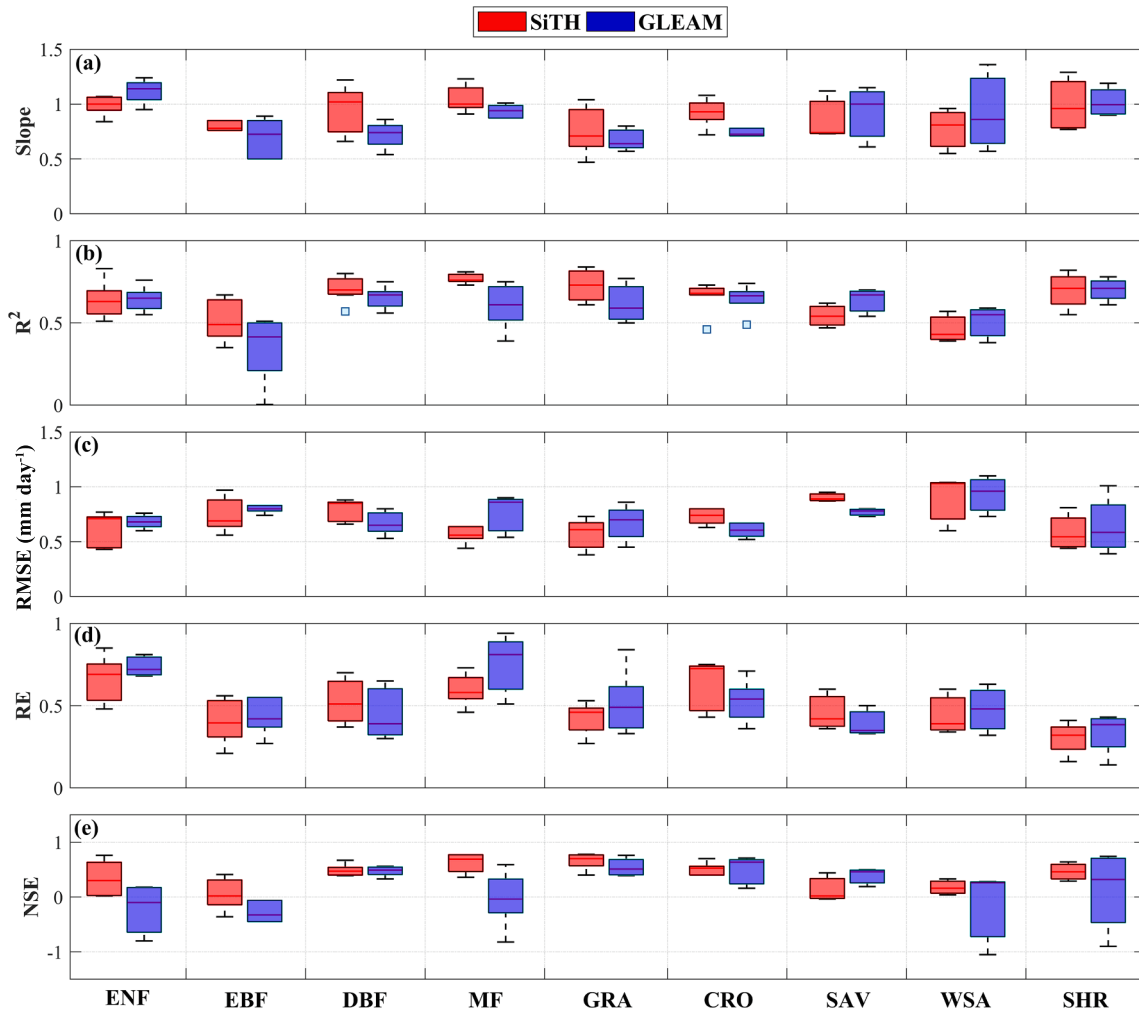


**Fig. 2.** Comparison between ET estimation of two models and tower measurements for the 46 sites scale across 9 biomes. Boxplots show the (a) slope, (b)  $R^2$ , (c) RMSE, (d) RE and (e) NSE statistical significance of simulated ET. The bottom and top of boxes mark the 25th and 75th percentiles, respectively. The central solid line of each box shows the median values.

Advanced Very High Resolution Radiometer (AVHRR) and Moderate Resolution Imaging Spectroradiometer (MODIS) satellite data, and it can be accessed from <http://www.globalmapping.org/>. Similar to GLEAM, we also selected the latest ERA-5 datasets as the forcing data (Hersbach and Dee, 2016). This datasets span from 1982 to 2017 at a 0.25°C spatial resolution and an hour temporal resolution, and are produced by European Centre for Medium-Range Weather Forecast (ECMWF) (<https://cds.climate.copernicus.eu/>). In addition, the static land cover data from MCD12C1 in 2001 was used as one of inputs (Friedl et al., 2010), because its changes were relatively small at a global scale over time (Zhang et al., 2016).

Because the input datasets vary in spatial resolution, we resampled them to a common 0.25° spatial resolution before using them as the forcing values. In addition, we performed temporal interpolation for LAI data set based on the nearest interpolation method to obtain daily data for the pixels.

### 2.3.2. Validation data

For site-scale comparisons, we selected a total of 46 flux sites from the FLUXNET database (<https://fluxnet.fluxdata.org>) to evaluate the performances of two models in ET simulations. For the purpose of validation, each flux site meets the following criteria: (1) more than one years of daily data available (not gap fill eddy covariance data). (2) mostly homogeneous land cover at 1 km radius from the flux tower (checked with Google Earth), and the land cover at sites location

matches with its in MCD12C1. (3) daily energy balance closure ranging from 0.70 to 0.95 (Supplementary Fig. S1). These 46 sites can be divided into 9 different vegetation types: evergreen needleleaf forests (ENF, 5 sites), evergreen broadleaf forests (EBF, 6 sites), deciduous broadleaf forests (DBF, 7 sites), mixed forests (MF, 5 sites), grasslands (GRA, 7 sites), croplands (CRO, 6 sites), savannas (SAV, 3 sites), wooden savannas (WSA, 3 sites), and shrublands (SHR, 4 sites). The map of all sites location and detailed information of all sites are shown in Fig. 1 and Table 1, respectively. In addition, field observations of the different components of ET (transpiration, soil evaporation and interception) were collected from published literatures (see details in Table 2). Noticeably, only one or two components of ET were directly measured at most sites, and the others were calculated by models using observed meteorological data or water balance methods. Here, only the direct measurements of the ET components were used for model performance comparisons.

For regional-scale comparison, the water balanced-ET datasets (WB-ET) for 32 major (i.e. >200,000 km<sup>2</sup>) catchments produced by Pan et al. (2012) were used to evaluate the model performance at catchment scales. These datasets were widely used to evaluate model performance at regional scale (Li et al., 2013; Wang et al., 2015), which include monthly precipitation, ET, streamflow, and the change in water storage from 1984 to 2006. The detailed information of 32 catchments were given in Supplementary Table S1 (Chen et al., 2020). In addition, the Model tree ensembles (MTE) product (Jung et al., 2009), which spans from

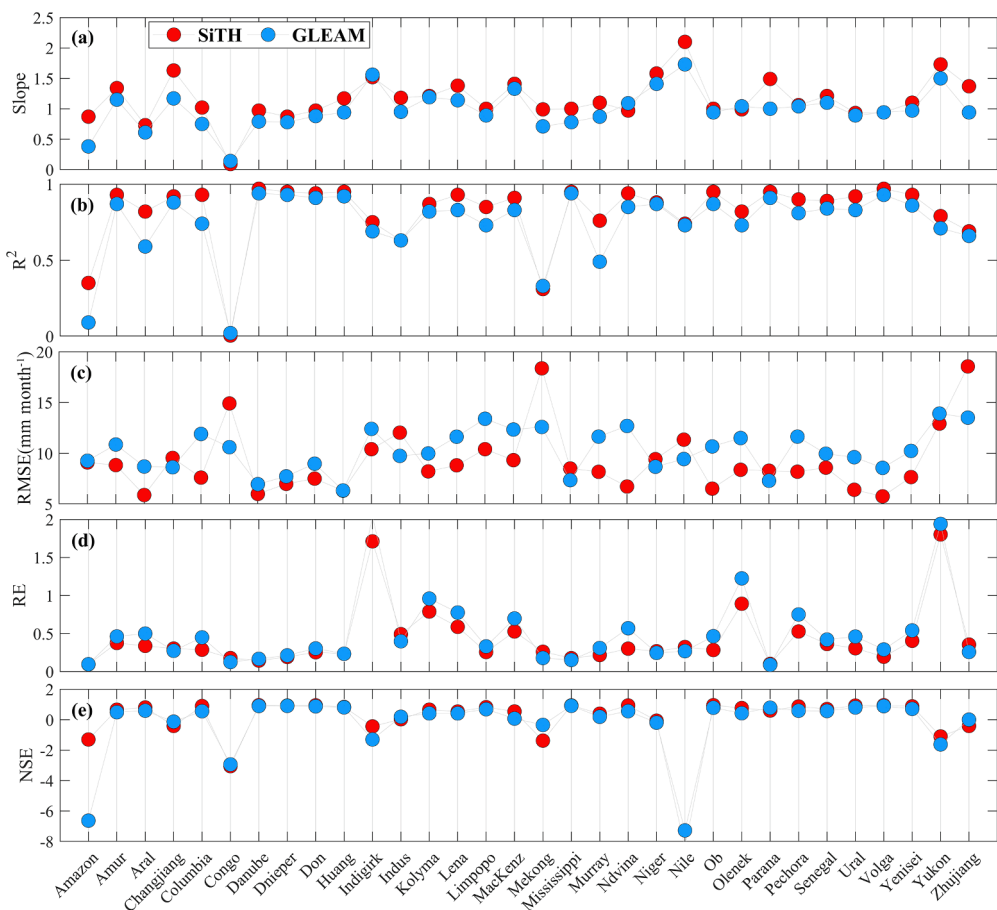


**Fig. 3.** Comparison of ET estimation of two models versus the water balanced-ET (WB-ET) at regional scale across 32 catchments. Figure shows the (a) slope, (b)  $R^2$ , (c) RMSE, (d) RE and (e) NSE statistical significance of simulated ET.

1982–2011 at monthly temporal and 0.5° spatial resolutions, was used for to evaluate the model performances at tropical rainforest. The MTE product is generated by using the machine-learning algorithm based on the ET observations from the FLUXNET data and remote sensing and meteorological data. All input and validation datasets are summarized in [Supplementary Table S2](#).

### 3. Results

#### 3.1. Performances of two models in total ET simulations at multiple scales

The five selected statistical measures (Slope,  $R^2$ , RMSE, RE and NSE) are used to evaluate the performance of two models at the 46 selected sites ([Fig. 2](#)) and 32 catchments ([Fig. 3](#)). At site scale, the average slopes between the simulated and observed ET ranged from 0.75 (GRA) to 1.05 (MF) for SiTH and from 0.69 (GRA) to 1.12 (ENF) for GLEAM, respectively. The SiTH and GLEAM displayed a similar range of mean RMSE values across all biomes (SiTH: RMSE = 0.59–0.90 mm day<sup>-1</sup>; GLEAM: RMSE = 0.64–0.93 mm day<sup>-1</sup>). The average values of RE ranged from 0.30 (SHR) to 0.66 (ENF) for SiTH and from 0.34 (SHR) to 0.75 (MF) for GLEAM. In addition, the average values of  $R^2$  ranged from 0.46 (WSA) to 0.77 (MF) for SiTH and from 0.34 (EBF) to 0.70 (SHR) for GLEAM. The SiTH produced slightly higher mean  $R^2$  values than that for GLEAM at most biomes, except for the SAV and WSA. Noticeably, relatively low  $R^2$  value for GLEAM were found at EBF sites from 0.004 to 0.51, indicating a poor consistency between the simulated and observed ET at these sites. Finally, the average NSE values for SiTH were greater than 0 over all biomes (0.08–0.65), which shows a greater consistency with the observed ET. However, the mean NSE values produced by GLEAM were

lower than 0 over some biomes, especially at EBF biome (NSE = -0.23).

At regional scale ([Fig. 3](#)), the slopes of regression between simulated ET by the two models and the estimated WB-ET were close to 1 at most basins. Nevertheless, its slope values were obviously higher than 1 at some catchments (i.e. Changjiang, Huang, Niger, Nile, and Yukon) and lower than 0.5 at Amazon and Congo basins. The  $R^2$  values for both models were higher than 0.6, except for some basins in tropic areas with  $R^2$  values less than 0.35 (i.e. Amazon, Congo and Mekong basins). Generally, the SiTH produced a slightly higher  $R^2$  values than that of GLEAM at all basins. In addition, the values of RMSE for SiTH were lower than that for GLEAM in most basins with the exceptions of Congo, Mekong, Zhujiang, Changjiang, Indus and Nile. The RE values for SiTH were slightly lower than that of GLEAM, which ranged from 0.10 (Amazon) to 1.80 (Yukong) for SiTH and from 0.10 (Amazon) to 2.04 (Indigirk) for GLEAM. The NSE values for SiTH were slightly greater than that for GLEAM at most basins, and two models generated NSE values greater than 0 except for the basins in tropics, Yukon, and Indigirk.

#### 3.2. The seasonal variations of ET in two models at different scales

We further analyzed the seasonal variations of ET from the two models at 46 sites. Generally, it was found that the seasonal patterns of ET were well captured by the two models at all sites (the selected 24 sites shown in [Supplementary Fig. S2](#)). However, at BR-Sa1 site, the seasonal variations of ET estimations by GLEAM showed difference with that of observations ([Fig. 4](#)). In addition to BR-Sa1 site, we also selected the BR-Sa3 site (3.02°S, 54.97°W) from FLUXNET data, and K34 site (2.60°S, 60.20°W) in the literature of [Da Rocha et al. \(2009\)](#) to further analyze

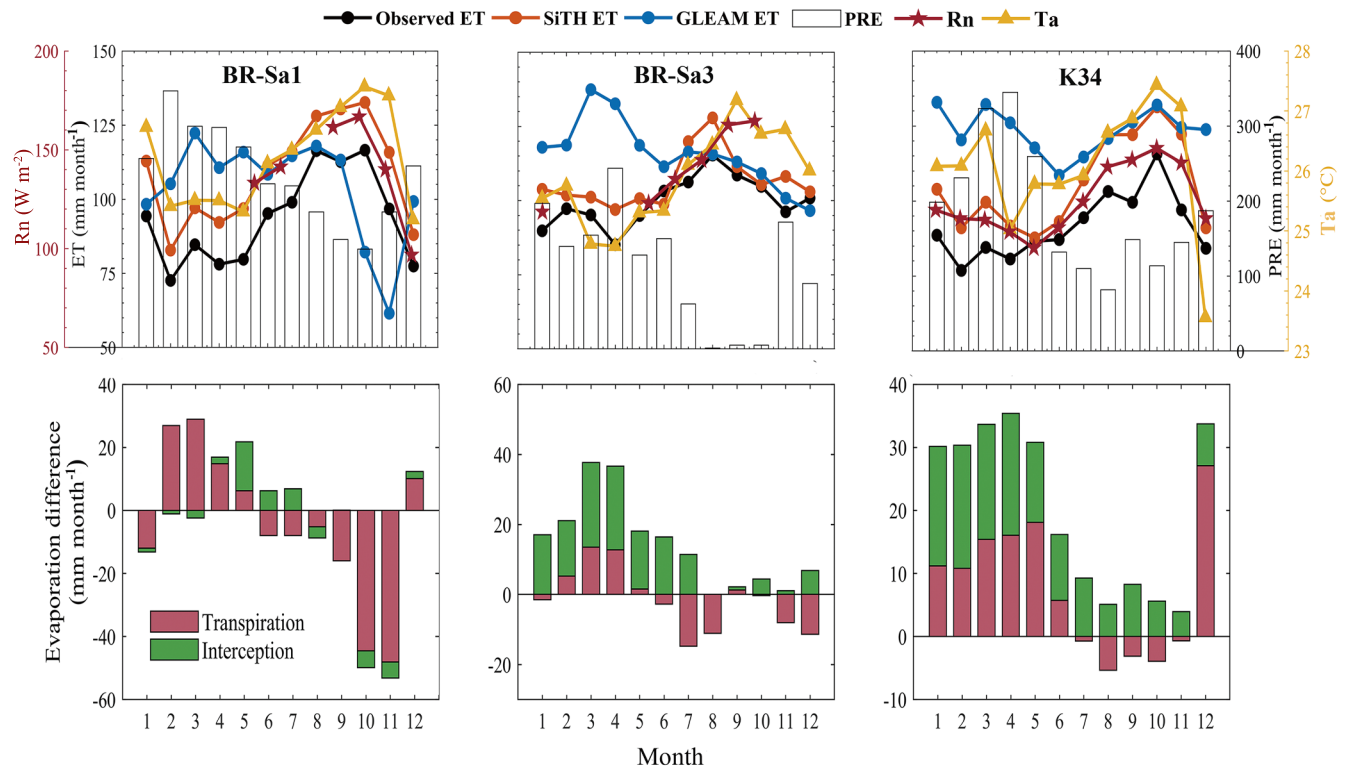


**Fig. 4.** The seasonal patterns of ET, precipitation (PRE), net radiation (Rn), air temperature (Ta), and estimated ET components at three tropical rainforest sites. The top panels represent the seasonal distribution of ET and PRE, Rn and Ta at BR-Sa1, BR-Sa3 and K34 sites, respectively. The bottom panels show the difference of mean per-month transpiration and interception between GLEAM and SiTH at BR-Sa1, BR-Sa3 and K34 sites, respectively.

the seasonal patterns of ET in tropical rainforest. The data at BR-Sa3 site in 2002 and 2004 and K34 from 1999 to 2006 were collected in this study. The mean annual precipitation over these sites were large (2701 mm year<sup>-1</sup> for BR-Sa1, 1569 mm year<sup>-1</sup> for BR-Sa3, and 2286 mm year<sup>-1</sup> for K34). Interestingly, the observed ET at three sites in the dry seasons were higher than that in wet seasons. The seasonal variations of observed ET at three sites were consistent with that of net radiation and temperature, but contrary to that of precipitation (Fig. 4). We found that the seasonal patterns of simulated ET by SiTH were generally consistent with that of the observed ET at the three sites. On the contrary, the seasonal patterns of simulated ET by GLEAM at these sites were different from that of observations with high values in wet seasons and low values in dry seasons. In addition, we also compared the different components of ET from two models at these sites (Fig. 4). It was found that during the wet seasons the interception loss and transpiration simulated by GLEAM were obviously higher than that simulated by SiTH. During dry seasons, the performances of the two models were comparable in the partitioning of ET at these sites.

In addition, long-term monthly average ET from 1984 to 2006 in SiTH and GLEAM versus the estimated WB-ET at 32 catchments were shown in Fig. 5. The seasonal patterns of estimated ET by SiTH and GLEAM were basically consistent with that of WB-ET at most of basins, with high values in local summer and low values in local winter. However, the simulated monthly average ET by the two models showed poor agreement with the estimated WB-ET over the basins in tropical regions (i.e. Amazon, Congo, and Mekong basins). In addition, the estimated ET by SiTH and GLEAM were slightly higher than the monthly average WB-ET at some basins, especially in Nile, Indigirk, and Yukon basins.

### 3.3. Performances of two models in the partitioning of ET at multiple scales

The estimated ET and its components by the two models against the

field measurements at each site were shown in Fig. 6. Generally, the performances of the two models in simulating total ET were similar. The slope of linear regression between observed and simulated ET was 0.99 and 1.05 for SiTH and GLEAM, respectively. The values of  $R^2$  were relatively high for the two models, being 0.84 and 0.80 for SiTH and GLEAM, respectively (Fig. 6d). However, the performances of the two models exhibited great differences in ET partitioning. The slopes of linear regression between observed and simulated transpiration were 0.98 and 1.51 for SiTH and GLEAM, respectively, suggesting that GLEAM tended to overestimate transpiration. Nevertheless, GLEAM produced a higher values of  $R^2$  for transpiration than SiTH (SiTH:  $R^2 = 0.51$ ; GLEAM:  $R^2 = 0.78$ ) (Fig. 6c). Additionally, the soil evaporation was significantly underestimated by GLEAM, with low values of the linear regression slope (0.02) and  $R^2$  (0.004). On the contrary, the SiTH performed relatively well in simulating soil evaporation (slope = 0.76 and  $R^2 = 0.62$ ) (Fig. 6a). For interception, we found that the two models tended to underestimate it with the values of regression slopes lower than 1 (0.40 and 0.55 for SiTH and GLEAM, respectively), despite with relatively high  $R^2$  (0.95 and 0.83 for SiTH and GLEAM, respectively) (Fig. 6b).

The spatial patterns of mean annual ET and its different components estimated by SiTH and GLEAM were shown in Fig. 7, and the fractions of transpiration, soil evaporation, and interception in total ET of the two models were shown in Fig. 8. The transpiration was the dominant component, accounting for 0.67 and 0.76 of total ET for SiTH and GLEAM, respectively. The estimated transpiration by GLEAM was generally higher than that by SiTH, and thus the ratios of transpiration to ET (that is,  $T_r/ET$ ) of GLEAM were apparently higher than that of SiTH at most regions, especially in low vegetation cover regions (i.e. shrublands and grasslands). Generally, low  $E_s$  values were estimated by these two models over dense vegetation areas, and high  $E_s$  values over biomes with low vegetation covers. However, the simulated soil evaporation and the ratio of soil evaporation to ET (that is,  $E_s/ET$ ) by SiTH (0.25)

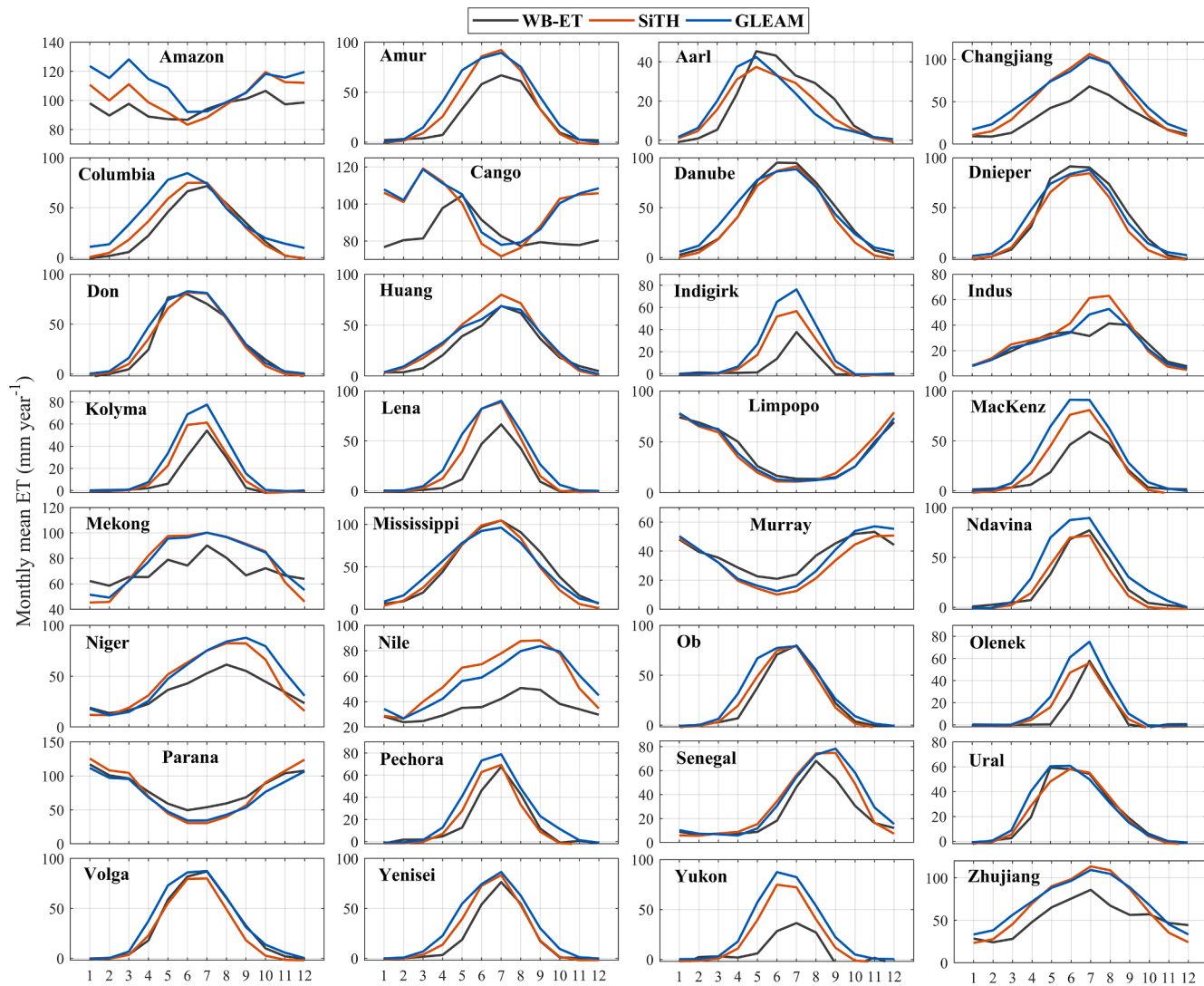


**Fig. 5.** Comparison of seasonal patterns of simulated ET of two models versus the water balanced-ET (WB-ET) at regional scale across 32 catchments.

were significantly higher than that estimated by GLEAM (0.09). Finally, the ratios of interception to ET (that is,  $E_i/ET$ ) by GLEAM (0.15) was slightly higher than that by SiTH (0.08), although the two models exhibited a consistent spatial distribution.

We also compared the performance of those two models in partitioning ET across different biomes (Table 3). The average  $T_r/ET$  ratios across different biomes estimated by GLEAM exhibited a relatively narrow range, varying from 0.60 (ENF) to 0.85 (CRO). On the contrary, the  $T_r/ET$  ratios estimated by SiTH showed large variations across different vegetation types, ranging from 0.32 (OSH) to 0.80 (WSA). Generally, the  $T_r/ET$  ratios estimated by GLEAM were clearly higher than that by SiTH over the SHR, GRA and CRO biomes (0.64–0.85 for GLEAM, and 0.32–0.64 for SiTH). The  $E_s/ET$  ratios estimated by GLEAM were lower than that estimated by SiTH across all biomes (0.01–0.30 for GLEAM, and 0.04–0.67 for SiTH). Noticeably, it is expected that the  $E_s/ET$  ratios over biomes with low vegetation covers should be high. However, the estimated  $E_s/ET$  ratios over these biomes by GLEAM were relatively low (0.12–0.30), and the estimated  $E_s/ET$  ratios by SiTH seemed to be in reasonable ranges (0.48–0.67). The estimated  $E_i/ET$  ratios for two models were high in forests, especially at tropical rainforest, and low in non-forest regions. Nevertheless, the estimated  $E_i/ET$  ratios by GLEAM were slightly higher than SiTH across all biomes, ranging from 0.03 to 0.29 for GLEAM and from 0.01 to 0.21 for SiTH, respectively.

## 4. Discussion

### 4.1. The global land ET anomalies in El Niño and La Niña events

It has been well documented that the ET over tropical rainforest was mainly determined by the energy rather than precipitation (Nemani et al., 2003; Jung et al., 2010; Zhang et al., 2016; Baker et al., 2021). Thus, increased radiation in dry seasons can produce greater ET than in wet seasons (Fig. 4). However, the seasonal variations in ET estimated by GLEAM were quite different from the observations. Thus, it seems that GLEAM can not properly capture the dynamics of ET in response to climate perturbations across the tropics. To verify our hypothesis, we analyzed inter-annual variability of ET (Fig. 9) and meteorological variables (Fig. 10) during typical El Niño (i.e. 1987, 1992, 1994 and 2002) and La Niña years (i.e. 1999, 2000, 2010, and 2011). The spatial patterns of ET estimated by GLEAM across tropics were significantly different from that estimated by SiTH and MTE product. During El Niño years, negative ET anomalies were found by GLEAM across the tropics, while positive anomalies were observed by SiTH and MTE. During La Niña years, the results were contrary to the above (Fig. 9). In addition, the spatial patterns of ET anomalies by SiTH and MTE are basically consistent with that of net radiation anomalies, while these by GLEAM displayed an agreement with that of precipitation in El Niño and La Niña years (Figs. 9 and 10). Recently, Purdy et al. (2018) also found increases

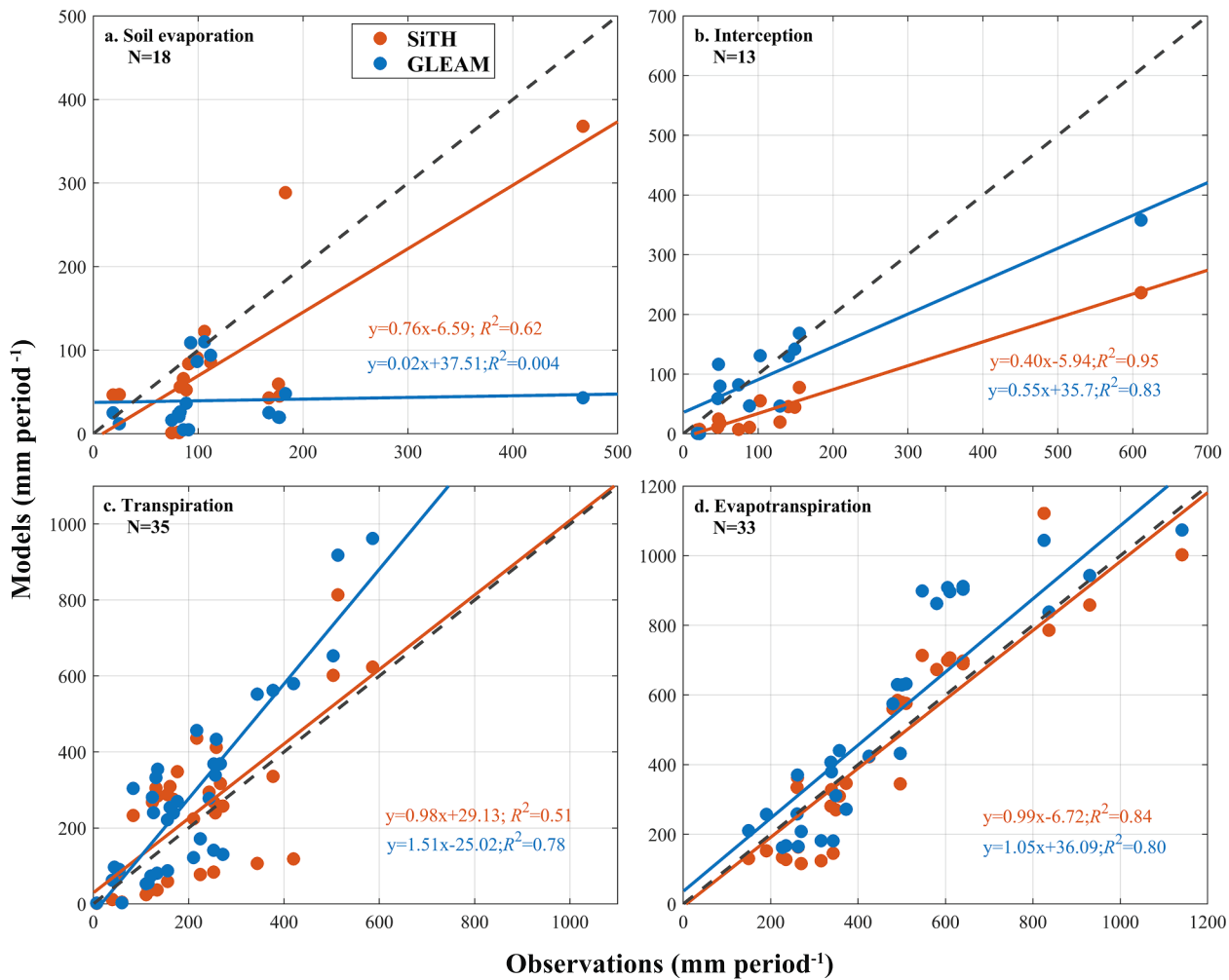


**Fig. 6.** Comparison between the estimated ET and its components of two models and field observations. Figure shows the linear regression between the modeled estimations and observed estimations for (a) soil evaporation, (b) interception, (c) transpiration, and (d) evapotranspiration, respectively.

in ET across the tropics during El Niño years by using an updated PT-JPL ET algorithm. Yan et al. (2013) noticed that positive ET anomalies in El Niño years and negative ET anomalies in La Niña years were occurred in tropics, and its spatial distribution was also consistent with potential ET, contrary to that of precipitation. Moreover, Guan et al. (2015) found that when annual rainfall was greater than 2000 mm year<sup>-1</sup>, the tropical rainforest can utilize the water storage from the wet season to satisfy the plant water demand. Thus, these two models exhibited contrasting behaviors and further exploration into the controlling mechanisms of ET are still needed across these regions.

#### 4.2. The uncertainty of model structure in ET partitioning

Generally, the daily variations of estimated ET by the two models showed a good consistency with the observations. Thus, these two models performed well in response to the changes in environmental factors (Supplementary Fig. S3). However, they exhibited great differences in ET partitioning due to differences in model structure and parameterization. The estimated soil evaporation by GLEAM was significantly lower than observations with relatively low regression slope and  $R^2$ . On the contrary, SiTH performed relatively well in simulations of soil evaporation with regression slope close to 1 and relatively high  $R^2$  (Fig. 4). In the two models, soil evaporation was constrained to occur only in the upper soil layer, and was tuned down to actual values by using similar stress functions (Eqs. (4 and 12) for GLEAM and SiTH, respectively). The main differences between them may be due to the

spatial grid representation of the ET processes. In the GLEAM model, soil evaporation under the tall and short canopy was ignored, and only takes the portion of bare soil in each grid into account (Eqs. 1 and 2). For the vegetation with low leaf area index, the soil evaporation under the vegetation canopy often contributed a significant portion of total ET (Black and Kelliher, 1989; Baldocchi and Meyers, 1991; Barbour et al., 2005; Unsworth et al., 2004). Thus, the underestimation of soil evaporation from GLEAM may occur in vegetated regions, especially over biomes with low vegetation covers (i.e. shrublands and grasslands).

Both models used soil water content as one of the stress factor to limit the potential transpiration. As the source of water for transpiration mainly comes from the soil, incorporating soil water content into the algorithms of transpiration can improve the model performances (Federer et al., 2003; Maurer et al., 2002; De Jeu et al., 2008; Purdy et al., 2018; Brust et al., 2021). However, these two models adopted different stress factors to reflect the vegetation state, such as plant temperature (Eq. (11)) for SiTH and vegetation optical depth (Eq. (3)) for GLEAM. However, the stress factor using temperature ( $f_T$ ; Eq. (11)) by SiTH may not well capture the actual vegetation state during the whole growing stages. On the contrary, VOD can reflect the plant water status as well as photosynthetic activity, and thus provides a dynamic information on vegetation state (Woodhouse, 2005; Liu et al., 2013; De Jeu et al., 2008; Miralles et al., 2011). Therefore, GLEAM can better capture the dynamic features of transpiration than SiTH (Fig. 6). In addition, in regions with sufficient water supply, ET was mainly determined by the atmospheric moisture demand (i.e. net radiation and vapour pressure deficit, which

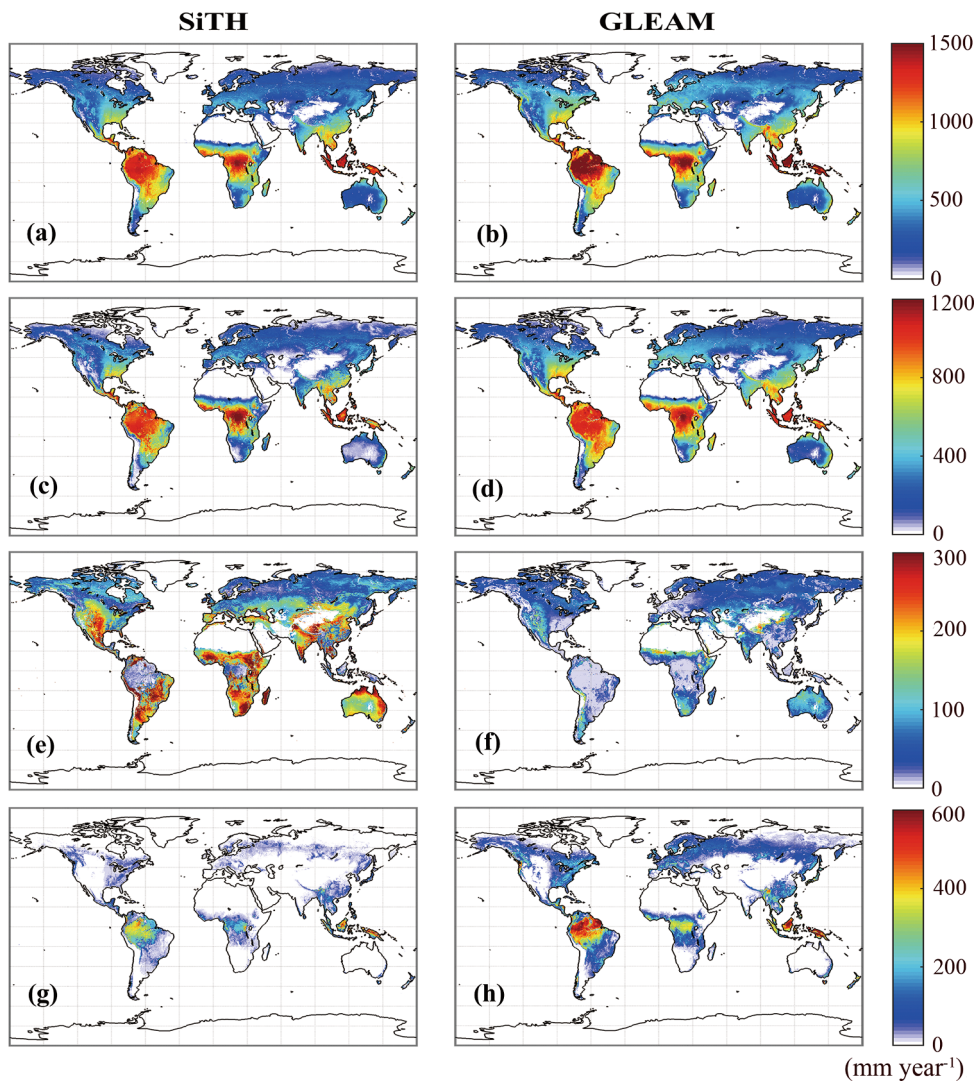


**Fig. 7.** Annual mean values over 1982–2017 of (a, b) ET and ET components: (c, d) transpiration, (e, f) soil evaporation, and (g, h) interception. The left and right panels show the estimated ET and its components in SiTH and GLEAM, respectively.

are often closely related with temperature) (Jung et al., 2010). Thus, the poor performances of GLEAM in energy-limited regions, such as tropical rainforest, may be due to the absence of stress factors of atmospheric moisture demand (which usually highly correlated with temperature). For SiTH, the overestimated ET in these regions may be due to the unconsidered influences of vegetation states on ET (Eq. (11)). Therefore, the stresses on transpiration should take the available soil moisture, vegetation state, and atmospheric moisture demand into accounts.

Interception loss is the process of the rainfall intercepted and stored by canopy, and subsequently lost by evaporation from the canopy. Thus, interception loss is strongly correlates with the amount of precipitation and canopy state (Pykner et al., 2005; Zheng and Jia, 2020). Although the estimated  $E_i$  by the two models showed a high correlation with field observations, these two models clearly underestimated interception loss, especially the SiTH model. Generally, GLEAM provided a slightly better estimates of  $E_i$  than SiTH. Up to date, filed observations of interception have been widely conducted. However, these were mainly concentrated on forest ecosystems, with few observations in sparse vegetation (Miralles et al., 2010; Zheng and Jia, 2020). Therefore, the specific source of uncertainty of two models in interception estimates was still unknown, and more filed observations are needed to understand mechanism of interception loss over sparse vegetation.

#### 4.3. Partitioning of ET into three components

Recently, researches on the  $T_r/ET$  ratio had attracted much attentions. For examples, Jasechko et al. (2013) reported that the transpiration accounted about 0.80–0.90 of ET based on isotope analysis across the global large basins. Taking the uncertainties of the isotopic data into accounts, Coenders-Gerrits et al. (2014) reported that the  $T_r/ET$  ratio ranged from 0.35 to 0.80. Good et al. (2015) estimated the ratios of  $T_r/ET$  being  $0.64 \pm 0.13$  based on atmospheric vapour isotope measurements and isotope mass budget. By compiling 81 filed observations, Schlesinger and Jasechko (2014) reported that the ratio of  $T_r/ET$  was about  $0.61 \pm 0.15$ . The results from land surface models had shown that the ratio of  $T_r/ET$  was only 0.43, and was argued to be underestimated (Lawrence et al., 2007, 2011; Wang-Erlandsson et al., 2014; Berg and Sheffield, 2019). Using the observations to constrain the land surface models, Lian et al. (2018) increased the estimated  $T_r/ET$  ratios from  $0.41 \pm 0.11$  to  $0.62 \pm 0.06$ . Recently, a global mean ratio of  $T_r/ET$  was estimated to be  $0.57 \pm 0.07$  based on 108 ensemble members from the combination of models and LAI-observed regression (Wei et al., 2017). In addition, many remote sensing-based models (PML and PT-JPL) estimated that the ratios of  $T_r/ET$  ranged from 0.54 to 0.65 (Purdy et al., 2018; Zhang et al., 2016). These indicated that the estimated  $T_r/ET$  ratio by SiTH (0.67) was closer to reported values than that estimated

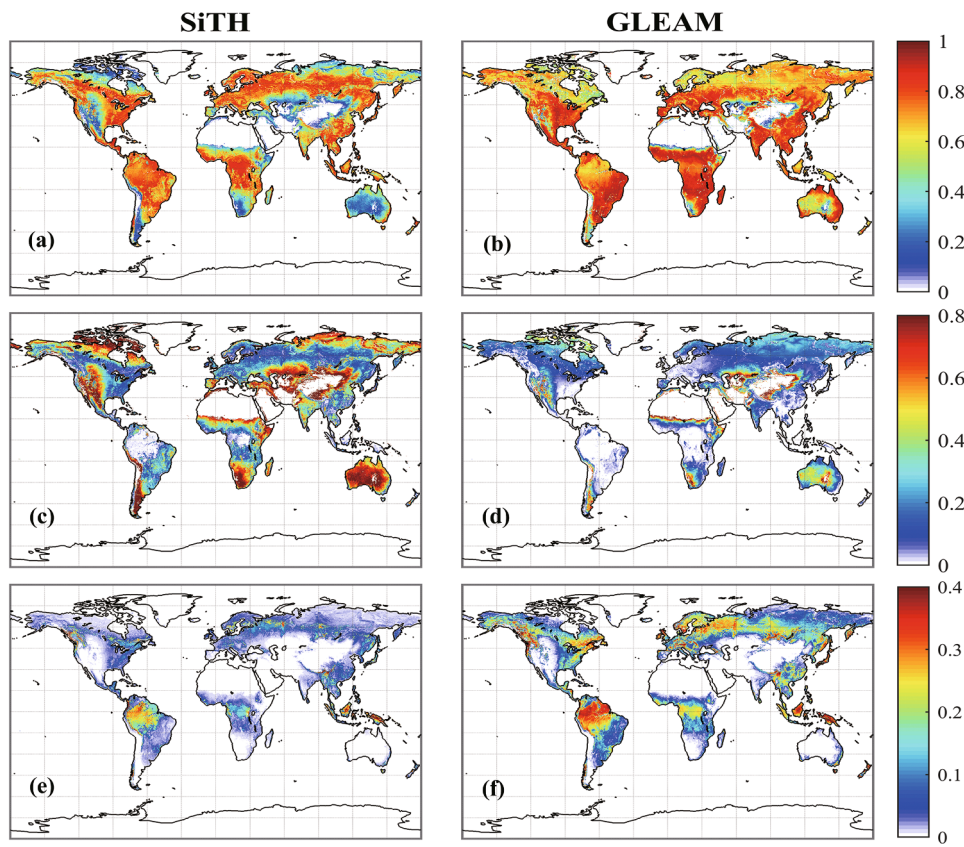


**Fig. 8.** Annual mean values over 1982–2017 of ratios of (a, b) transpiration, (c, d) soil evaporation, and (e, f) interception to total ET. The left and right panels show the ET partitioning in GLEAM and SiTH, respectively.

**Table 3**

Comparison of ET partitioning in two models across different biome.

Vegetation	$T_r/ET$		$E_s/ET$		$E_i/ET$	
	GLEAM	SiTH	GLEAM	SiTH	GLEAM	SiTH
ENF	0.60	0.65	0.04	0.15	0.29	0.21
EBF	0.72	0.76	0.01	0.04	0.24	0.20
DNF	0.72	0.70	0.09	0.17	0.17	0.12
DBF	0.78	0.76	0.02	0.17	0.18	0.07
MF	0.68	0.76	0.04	0.14	0.24	0.10
CSH	0.78	0.47	0.12	0.52	0.04	0.01
OSH	0.64	0.32	0.30	0.67	0.03	0.01
WSA	0.76	0.80	0.03	0.15	0.16	0.05
SAV	0.84	0.73	0.03	0.24	0.09	0.03
GRA	0.79	0.51	0.14	0.48	0.03	0.01
CRO	0.85	0.64	0.07	0.35	0.04	0.02

by GLEAM (0.76). The overestimation of  $T_r/ET$  ratio for GLEAM mainly occurred in GRA (0.79), CRO (0.85), and CSH (0.78), compared with the mean  $T_r/ET$  values being around  $0.51 \pm 0.15$  across these biome in previous studies (Lauenroth and Bradford, 2006; Alton et al., 2009; Schlesinger and Jasechko, 2104; Wang-Erlansson et al., 2014; Zhou et al., 2016; Gu et al., 2018; Sun et al., 2019; Xu, et al., 2021).

At global, the  $E_s/ET$  ratio in SiTH (0.25) was greater than GLEAM (0.09), and the  $E_i/ET$  ratio in SiTH (0.08) was lower than GLEAM (0.15). At present, the model-based global mean  $E_s/ET$  ratios were estimated to range from 0.24 to 0.52 (Miralles et al., 2016; Purdy et al., 2018; Dirmeyer et al., 2005; Berg and Sheffield, 2019). These results may indicate that GLEAM tended to underestimate the ratios of  $E_s/ET$ . Over low vegetation regions, relative low  $E_s/ET$  ratios were estimated by GLEAM (i.e. 0.14 for GRA and 0.12 for CSH). However, direct observations showed that soil evaporation may account 0.50 of total ET compared over these regions (Wang-Erlansson et al., 2014; Zhou et al., 2016). For

canopy interception, the global mean  $E_i/ET$  ratios were generally estimated ranging from 0.10 to 0.24 (Dirmeyer et al., 2005; Zhang et al., 2016; Miralles et al., 2016). These results indicate that SiTH slightly underestimated the  $E_s/ET$  ratio. However, the exact ratios of soil evaporation and canopy interception to ET at global scale are still lack.

## 5. Conclusion

Using remote sensing ET models for GLEAM and SiTH based on the Priestley-Taylor equation, this study systematically evaluated ET partitioning and the uncertainty of ET partitioning in the model structure. In general, both two models in ET simulations performed well at different scales, except the poor performance of GLEAM occurring in tropical rainforest. Lack of the stress of atmospheric moisture demand on transpiration in GLEAM, lead to the overestimation of ET in wet seasons at tropical rainforest. As for the ET partitioning, the overestimated

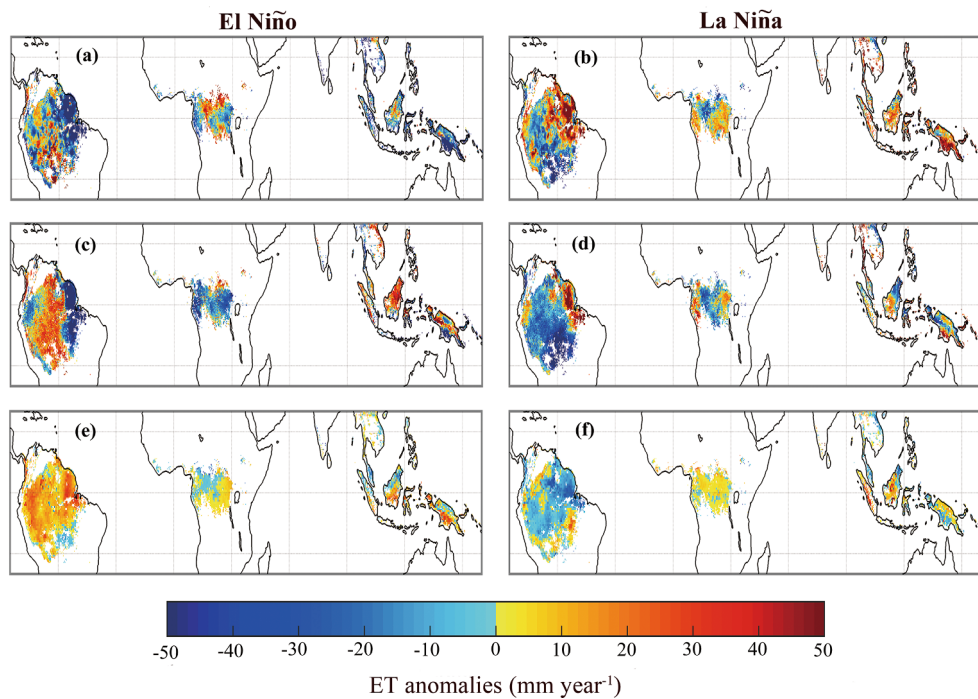


**Fig. 9.** Spatial patterns of ET annual anomalies in (a, b) GLEAM, (c, d) SiTH and (e, f) MTE at tropical rainforest during El Niño and La Niña events. The left and right panels show the ET annual anomalies during El Niño and La Niña years, respectively.

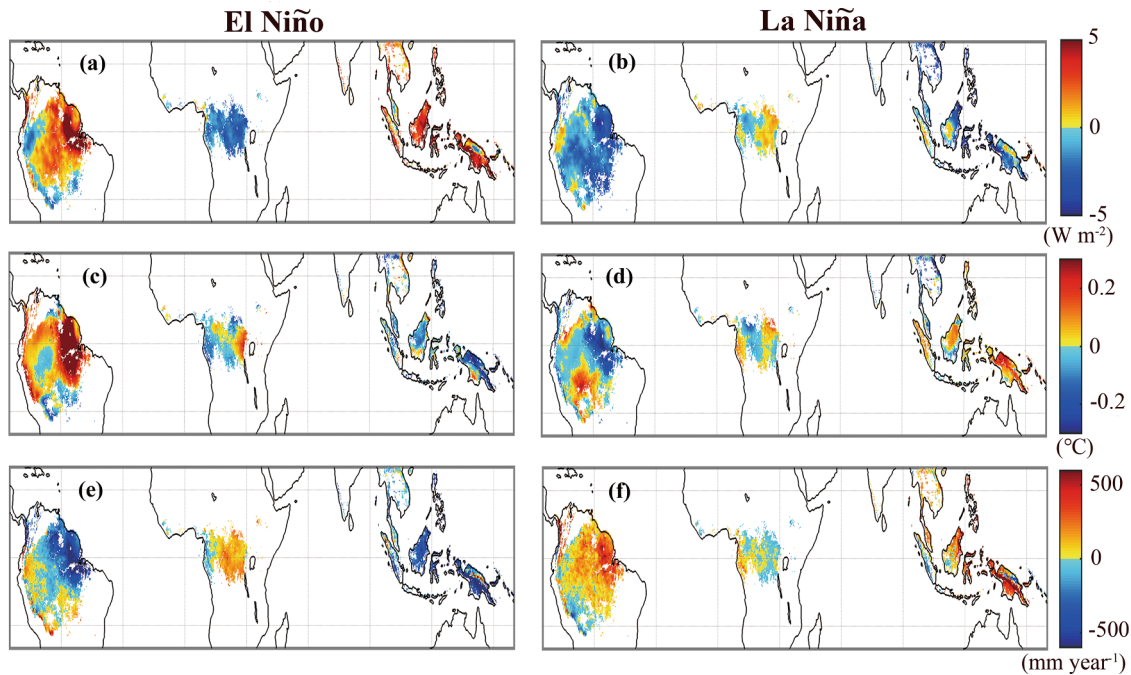


**Fig. 10.** Spatial patterns of annual anomalies for (a, b) net radiation, (c, d) air temperature and (e, f) precipitation at tropical rainforest during El Niño and La Niña events. The left and right panels show the annual anomalies during El Niño and La Niña years, respectively.

transpiration and slightly underestimated interception were occurred in GLEAM, and modeled soil evaporation showed poor performance with the filed observations. Comparing with the observations, the SiTH performed relatively well in simulating soil evaporation, and underestimated interception. The modeled transpiration in SiTH provided a lower correlation with observations than GLEAM, owing to plant temperature limitation cannot reflect actual vegetation state. In addition, the  $T_r/ET$  ratio in GLEAM was 0.76 with values higher than that of SiTH

(0.67) and previous studies (central mean value around 0.60), and the  $E_s/ET$  values in GLEAM (0.09) was clearly lower than SITH (0.25) and other modeled values. Due to neglecting the soil evaporation under short and tall vegetation, results in the clearly overestimated  $T_r/ET$  ratio and underestimated  $E_s/ET$  in GLEAM occurred over low vegetation covers, with  $T_r/ET$  and  $E_s/ET$  values ranging from 0.64 to 0.85 and from 0.07 to 0.30, respectively. The modeled  $E_i/ET$  ratio in SiTH (0.08) was slightly lower than GLEAM (0.15).

The different scheme of parameterization of evaporation stress factors results in the different performance of models at ET partitioning. In this study, we figure out the source of uncertainties of two models in ET partitioning, therefore, improvements of ET partitioning, still needs more field observations to understand its mechanism and optimize the parameters and structure.

### CRediT authorship contribution statement

**Huiling Chen:** Writing – original draft, Conceptualization. **Gao Feng Zhu:** Writing – review & editing, Funding acquisition. **Shasha Shang:** Methodology. **Wenhua Qin:** Methodology. **Yang Zhang:** Formal analysis. **Yonghong Su:** Software, Funding acquisition. **Kun Zhang:** Funding acquisition, Software. **Yongtai Zhu:** Software, Funding acquisition, Data curation. **Cong Xu:** Data curation.

### Declaration of Competing Interest

The authors declare that they have no known competing financial interests or personal relationships that could have appeared to influence the work reported in this paper.

### Acknowledgements

This research is founded by the National Natural Science Foundation of China (Nos. 41871078, 42071138 and 41901381). We are grateful to the principal investigators and their teams of all the data set used in this study. This work used eddy covariance data acquired and shared by the FLUXNET community, including these networks: AmeriFlux, AfriFlux, AsiaFlux, CarboAfrica, CarboEuropeIP, CarboItaly, CarboMont, ChinaFlux, Fluxnet-Canada, GreenGrass, ICOS, KoFlux, LBA, NECC, OzFlux-TERN, TCOS-Siberia, and USCCC, available at <https://fluxnet.fluxdata.org>. The GLEAM datasets are available at <https://www.gleam.eu/>. The GLOBMAP datasets are available at <http://www.globalmapping.org/>. The ERA5 reanalysis datasets are acquired from <https://cds.climate.copernicus.eu/>. The MCD12C1 products used in this study are available at <https://lpdaac.usgs.gov/>. The MTE datasets are acquired from <http://www.bgc-jena.mpg.de/geodb/>.

### Appendix A. Supplementary data

Supplementary data to this article can be found online at <https://doi.org/10.1016/j.jhydrol.2021.127223>.

### References:

- Alton, P., Fisher, R., Los, S., Williams, M., 2009. Simulations of global evapotranspiration using semiempirical and mechanistic schemes of plant hydrology. *Global Biogeochem. Cy.* 23 (GB4032), 2009. <https://doi.org/10.1029/2009GB003540>.
- Anthoni, P.M., Knohl, A., Rebmann, C., Freibauer, A., Mund, M., Ziegler, W., Kolle, O., Schulze, E.D., 2004. Forest and agricultural land-use-dependent CO<sub>2</sub> exchange in Thuringia. Germany. *Glob. Chang. Biol.* 10 (12), 2005–2019. <https://doi.org/10.1111/j.1365-2486.2004.00863.x>.
- Archibald, S.A., Kirton, A., van der Merwe, M.R., Scholes, R.J., Williams, C.A., Hanan, N., 2009. Drivers of inter-annual variability in Net Ecosystem Exchange in a semi-arid savanna ecosystem. South Africa. *Biogeosciences*. 6 (2), 251–266. <https://doi.org/10.5194/bg-6-251-2009>.
- Aubinet, M., Chermantte, B., Vandenhaute, M., Longdoz, B., Yernaux, M., Laitat, E., 2001. Long term carbon dioxide exchange above a mixed forest in the Belgian Ardennes. *Agric. For. Meteorol.* 108 (4), 293–315. [https://doi.org/10.1016/S0168-1923\(01\)00244-1](https://doi.org/10.1016/S0168-1923(01)00244-1).
- Baker, J.C.A., Garcia-Carreras, L., Gloor, M., Marsham, J.H., Buermann, W., da Rocha, H.R., Nobre, A.D., de Araujo, A.C., Spracklen, D.V., 2021. Evapotranspiration in the Amazon: spatial patterns, seasonality, and recent trends in observations, reanalysis, and climate models. *Hydrol. Earth Syst. Sci.* 25, 2279–2300. <https://doi.org/10.5194/hess-25-2279-2021>.
- Baldocchi, D.D., Meyers, T.P., 1991. Trace gas exchange above the floor of a deciduous forest: 1. Evaporation and CO<sub>2</sub> flux. *J. Geophys. Res.* 96, 7271–7285. <https://doi.org/10.1029/91JD00269>.
- Baldocchi, D., Penuelas, J., 2018. The Physics And Ecology Of Mining Carbon Dioxide From The Atmosphere By Ecosystems. *Glob. Chang. Biol.* 301–302 (7), 108350. <https://doi.org/10.1111/gcb.14559>.
- Barbour, M.M., Hunt, J.E., Walcroft, A.S., Rogers, G.N.D., McSeveny, T.M., Whitehead, D., 2005. Components of ecosystem evaporation in a temperate coniferous rainforest, with canopy transpiration scaled using sap-wood density. *New Phytol.* 165, 549–558. <https://doi.org/10.1111/j.1469-8137.2004.01257.x>.
- Berg, A., Sheffield, J., 2019. Evapotranspiration partitioning in CMIP5 models: uncertainties and future projections. *J. Clim.* 32, 2653–2671. <https://doi.org/10.1175/JCLI-D-18-0583.s1>.
- Beringer, J., Hutley, L.B., Hacker, J.M., Neininger, B., Paw, U., K. T., 2011. Patterns and processes of carbon, water and energy cycles across northern Australian landscapes: From point to region. *Agric. For. Meteorol.* 151 (11), 1409–1416. <https://doi.org/10.1016/j.agrformet.2011.05.003>.
- Beringer, J., Hutley, L.B., McHugh, I., Arndt, S.K., Campbell, D., Cleugh, H.A., Cleverly, J., Resco de Dios, V., Eamus, D., Evans, B., Ewenz, C., Grace, P., Griebel, A., Haverd, V., Hinko-Najera, N., Huete, A., Isaac, P., Kanniah, K., Leuning, R., Liddell, M.J., Macfarlane, C., Meyer, W., Moore, C., Pendall, E., Phillips, A., Phillips, R.L., Prober, S.M., Restrepo-Coupe, N., Rutledge, S., Schroder, I., Silberstein, R., Southall, P., Yee, M.S., Tapper, N.J., van Gorsel, E., Vote, C., Walker, J., Wardlaw, T., 2016. An introduction to the Australian and New Zealand flux tower network – OzFlux. *Biogeosciences*. 13, 5895–5916. <https://doi.org/10.5194/bg-13-5895-2016>.
- Beringer, J., Hutley, L.B., Tapper, N.J., Cernusak, L.A., 2007. Savanna fires and their impact on net ecosystem productivity in North Australia. *Glob. Chang. Biol.* 13 (5), 990–1004. <https://doi.org/10.1111/j.1365-2486.2007.01334.x>.
- Black, T.A., Kelliher, F.M., 1989. Process controlling understorey evapotranspiration. *Phil. Trans. R. Soc. B* 324, 207–231. <https://doi.org/10.1098/rstb.1989.0045>.
- Bristow, M., Hutley, L.B., Beringer, J., Livesley, S.J., Edwards, A.C., Arndt, S.K., 2016. Quantifying the relative importance of greenhouse gas emissions from current and future savanna land use change across northern Australia. *Biogeosciences*. 13 (22), 6285–6303. <https://doi.org/10.5194/bg-13-6285-2016>.
- Brooks, J.R., Flanagan, L.B., Varney, G.T., Ehleringer, J.R., 1997. Vertical Gradients In Photosynthetic Gas Exchange Characteristics And Refixation Of Respired CO<sub>2</sub> Within Boreal Forest Canopies. *Tree Physiol.* 17 (1), 1–12. <https://doi.org/10.1093/treephys/17.1.1>.
- Brust, C., Kimball, J.S., Maneta, M.P., Jencso, K., He, M.Z., Reichle, R.H., 2021. Using SMAP Level-4 soil moisture to constrain MOD16 evapotranspiration over the contiguous USA. *Remote Sens. Environ.* 255, 112277. <https://doi.org/10.1016/j.rse.2020.112277>.
- Carrara, A., Janssens, I.A., Curiel Yuste, J., Ceulemans, R., 2004. Seasonal changes in photosynthesis, respiration and NEE of a mixed temperate forest. *Agric. For. Meteorol.* 126 (1–2), 15–31. <https://doi.org/10.1016/j.agrformet.2004.05.002>.
- Cavanaugh, M.L., Kurc, S.A., Scott, R.L., 2011. Evapotranspiration partitioning in semiarid shrubland ecosystems: a two-site evaluation of soil moisture control on transpiration. *Ecology*. 4, 671–681. <https://doi.org/10.1002/eco.157>.
- Cernusak, L.A., Hutley, L.B., Beringer, J., Holtum, J.A.M., Turner, B.L., 2011. Photosynthetic physiology of eucalypts along a sub-continental rainfall gradient in northern Australia. *Agric. For. Meteorol.* 151 (11), 1462–1470. <https://doi.org/10.1016/j.agrformet.2011.01.006>.
- Chen, H.L., Zhu, G.F., Zhang, K., Bi, J., Jia, X.P., Ding, B.Y., Zhang, Y., Shang, S.S., Zhao, N., Qin, W.H., 2020. Evaluation of evapotranspiration models using different LAI and meteorological forcing data from 1982 to 2017. *Remote Sens.* 12, 2473. <https://doi.org/10.3390/rs12152473>.
- Cleugh, H.A., Leuning, R., Mu, Q.Z., Running, S.W., 2007. Regional evaporation estimates from flux tower and MODIS satellite data. *Remote Sens. Environ.* 106, 285–304. <https://doi.org/10.1016/j.rse.2006.07.007>.
- Coenders-Gerrits, A.M.J., van der Ent, R.J., Bogaard, T.A., Wang-Erlandsson, L., Hrachowitz, M., Savenije, H.H.G., 2007. Uncertainties in transpiration estimates. *Natur* 506, E1–E2. <https://doi.org/10.1038/nature12925>.
- Da Rocha, H.R., Manzi, A.O., Cabral, O.M., Miller, S.D., Goudeau, M.L., Saleska, S.R., Coupe, N.R., Wofsy, S.C., Borma, L.S., Artaxo, R., Vourlitis, G., Nogueira, J.S., Cardoso, F.L., Nobre, A.D., Kruijt, B., Freitas, H.C., Von Randow, C., Aguiar, R.G., Maia, J.F., 2009. Patterns of water and heat flux across a biome gradient from tropical forest to savanna in Brazil. *J. Geophys. Res. Biogeosci.* 114, G00B12. <https://doi.org/10.1029/2007JG000640>.
- De Jeu, R.A.M., Wagner, W., Holmes, T.R.H., Dolman, A.J., van de Giesen, N.C., Friesen, J., 2008. Global soil moisture patterns observed by space borne microwave radiometers and scatterometers. *Surv. Geophys.* 29, 399–420. <https://doi.org/10.1007/s10712-008-9044-0>.
- Delpierre, N., Berveiller, D., Granda, E., Dufrêne, E., 2016. Wood phenology, not carbon input, controls the interannual variability of wood growth in a temperate oak forest. *New Phytol.* 210 (2), 459–470. <https://doi.org/10.1111/nph.13771>.
- Desai, A.R., Bolstad, P.V., Cook, B.D., Davis, K.J., Carey, E.V., 2005. Comparing Net Ecosystem Exchange Of Carbon Dioxide Between An Old-Growth And Mature Forest In The Upper Midwest. Usa. *Agric. For. Meteorol.* 128 (1–2), 33–55. <https://doi.org/10.1016/j.agrformet.2004.09.005>.
- Dirmeyer, P.A., Gao, X., Zhao, M., Guo, Z.C., Oki, T., Hanasaki, N., 2005. The second Global Soil Wetness Project (GSWP-2): Multi-model analysis and implications for our perception of the land surface. *COLA. Tech. Rep.* 185, 46 pp.
- Ershadi, A., McCabe, M.F., Evans, J.P., Chaney, N.W., Wood, E.F., 2014. Multi-site evaluation of terrestrial evaporation models using FLUXNET data. *Agric. For. Meteorol.* 187, 46–61. <https://doi.org/10.1016/j.agrformet.2013.11.008>.
- Federer, C.A., Vörösmarty, C., Fekete, B., 2003. Sensitivity of Annual Evaporation to Soil and Root Properties in Two Models of Contrasting Complexity. *J. Hydrometeorol.* 4 (6), 1276–1290. <https://doi.org/10.1175/1525-7541>.
- FERRETTI, D.F., PENDALL, E., MORGAN, J.A., NELSON, J.A., LECAIN, D., MOSIER, A.R., 2003. Partitioning evapotranspiration fluxes from a Colorado grassland using stable

- isotopes: seasonal variations and ecosystem implications of elevated atmospheric CO<sub>2</sub>. *Plant Soil.* 254, 291–303. <https://doi.org/10.1023/A:1025511618571>.
- Fisher, J.B., Tu, K.P., Baldocchi, D.D., 2008. Global estimates of the land-atmosphere water flux based on monthly AVHRR and ISLSCP-II data, validated at 16 FLUXNET sites. *Remote Sens. Environ.* 112, 901–919. <https://doi.org/10.1016/j.rse.2007.06.025>.
- Friedl, M.A., Sulla-Menashe, D., Tan, B., Schneider, A., Ramankutty, N., Sibley, A., Huang, X., 2010. MODIS Collection 5 global land cover: Algorithm refinements and characterization of new datasets. *Remote Sens. Environ.* 114, 168–182. <https://doi.org/10.1016/j.rse.2009.08.016>.
- Gash, J.H., Stewart, J.B., 1977. The evaporation from Thetford Forest during 1975. *J. Hydrol.* 35, 385–396. [https://doi.org/10.1016/0022-1694\(77\)90014-2](https://doi.org/10.1016/0022-1694(77)90014-2).
- Gash, J.H., 1979. An analytical model of rainfall interception by forests. *Q. J. Roy. Meteorol. Soc.* 105, 43–55. <https://doi.org/10.1002/qj.49710544304>.
- Good, S.P., Noone, D., Bowen, G., 2015. Hydrologic connectivity constrains partitioning of global terrestrial water fluxes. *Science* 349, 175–177. <https://doi.org/10.1126/science.aaa5931>.
- Granier, A., Biron, P., Lemoine, D., 2000. Water balance, transpiration and canopy conductance in two beech stands. *Agric. For. Meteorol.* 100 (4), 291–308. [https://doi.org/10.1016/S0168-1923\(99\)00151-3](https://doi.org/10.1016/S0168-1923(99)00151-3).
- Granier, A., Breda, N., Biron, P., Villette, S., 1999. A lumped water balance model to evaluate duration and intensity of drought constraints in forest stands. *Ecol. Model.* 116, 269–283. [https://doi.org/10.1016/S0304-3800\(98\)00205-1](https://doi.org/10.1016/S0304-3800(98)00205-1).
- Grelle, A., Lundberg, A., Lindroth, A., Morén, A.S., Cienciala, E., 1997. Evaporation components of a boreal forest: variations during the growing season. *J. Hydrol.* 197, 70–87. [https://doi.org/10.1016/S0022-1694\(96\)03267-2](https://doi.org/10.1016/S0022-1694(96)03267-2).
- Gu, C.J., Ma, J.Z., Zhu, G.F., Yang, H., Zhang, K., Wang, Y.Q., Gu, C.L., 2018. Partitioning evapotranspiration using an optimized satellite-based ET model across biomes. *Agric. For. Meteorol.* 259, 355–363. <https://doi.org/10.1016/j.agrformet.2018.05.023>.
- Guan, D.X., Wu, J.B., Zhao, X.S., Han, S.J., Yu, G.R., Sun, X.M., Jin, C.J., 2006. CO<sub>2</sub> fluxes over an old, temperate mixed forest in northeastern China. *Agric. For. Meteorol.* 137 (3–4), 138–149. <https://doi.org/10.1016/j.agrformet.2006.02.003>.
- Guan, K.Y., Pan, M., Li, H.B., Wolf, A., Wu, J., Medvigy, D., Taylor, K.K., Sheffield, J., Wood, E.F., Malhi, Y., Liang, M.L., Kimball, J.S., Saleska, S.R., Berry, J., Joiner, J., Lyapustin, A.I., 2015. Photosynthetic seasonality of global tropical forests constrained by hydroclimate. *Nature Geosci.* 8, 284–289. <https://doi.org/10.1038/ngeo2382>.
- Han, D.M., Wang, G.Q., Liu, T.X., Xue, B.L., Kuczera, G., Xu, X.Y., 2018. Hydroclimatic Response of Evapotranspiration Partitioning to Prolonged Droughts in Semiarid Grassland. *J. Hydrol.* 563, 766–777. <https://doi.org/10.1016/j.jhydrol.2018.06.048>.
- Hardiman, B.S., Bohrer, G., Gough, C.M., Vogel, C.S., Curtis, P.S., 2011. The Role Of Canopy Structural Complexity In Wood Net Primary Production Of A Maturing Northern Deciduous Forest. *Ecology.* 92 (9), 1818–1827. <https://doi.org/10.1890/10-2192.1>.
- Hersbach, H., Dee, D., 2016. ERA5 reanalysis is in production. *ECMWF Newsletter.* 147.
- Hölscher, D., Köhler, L., Van Dijk, A.I.J.M., Bruijnzeel, L.A., 2004. The importance of epiphytes to total rainfall interception by a tropical montane rain forest in Costa Rica. *J. Hydrol.* 292, 308–322. <https://doi.org/10.1016/j.jhydrol.2004.01.015>.
- Hutley, L.B., Beringer, J., Isaac, P.R., Hacker, J.M., Cernusak, L.A., 2011. A sub-continental scale living laboratory: Spatial patterns of savanna vegetation over a rainfall gradient in northern Australia. *Agric. For. Meteorol.* 151 (11), 1417–1428. <https://doi.org/10.1016/j.agrformet.2011.03.002>.
- Hymus, G.J., Johnson, D.P., Dore, S., Anderson, H.P., Ross Hinkle, C., Drake, B.G., 2003. Effects Of Elevated Atmospheric CO<sub>2</sub> On Net Ecosystem CO<sub>2</sub> Exchange Of A Scrub-Oak Ecosystem. *Glob. Chang. Biol.* 9 (12), 1802–1812. <https://doi.org/10.1111/j.1365-2486.2003.00675.x>.
- Iida, S., Tanaka, T., Sugita, M., 2006. Change of evapotranspiration components due to the succession from Japanese red pine to evergreen oak. *J. Hydrol.* 326, 166–180. <https://doi.org/10.1016/j.jhydrol.2005.11.002>.
- Iner, D., Merbold, L., Eugster, W., Buchmann, N., 2013. Temporal and spatial variations of soil CO<sub>2</sub>, CH<sub>4</sub> and N<sub>2</sub>O fluxes at three differently managed grasslands. *Biogeosciences.* 10 (9), 5931–5945. <https://doi.org/10.5194/bg-10-5931-2013>.
- Jasechko, S., Sharp, Z.D., Gibson, J.J., Birks, S.J., Yi, Y., Fawcett, P.J., 2013. Terrestrial water fluxes dominated by transpiration. *Nature.* 496, 347–350. <https://doi.org/10.1038/nature11983>.
- Jung, M., Reichstein, M., Ciais, P., Seneviratne, S.I., Sheffield, J., Goulden, M.L., Bonan, G., Cescatti, A., Chen, J., de Jeu, R., Dolman, A.J., Eugster, W., Gerten, D., Gianelle, D., Gobron, N., Heinke, J., Kimball, J., Law, B.E., Montagnani, L., Mu, Q., Mueller, B., Oleson, K., Papale, D., Richardson, A.D., Rouspard, O., Running, S., Tomelleri, E., Viovy, N., Weber, U., Williams, C., Wood, E., Zedler, S., Zhang, K., 2010. Recent decline in the global land evapotranspiration trend due to limited moisture supply. *Nature.* 467, 951–954. <https://doi.org/10.1038/nature09396>.
- Kool, D., Agam, N., Lazarovitch, N., Heitman, J.L., Sauer, T.J., Ben-Gal, A.A., 2014. Review of approaches for evapotranspiration partitioning. *Agric. For. Meteorol.* 184, 56–70. <https://doi.org/10.1016/j.agrformet.2013.09.003>.
- Kumar, S., Holmes, T., Mocko, D., Wang, S., Peters-Lidard, C., 2018. Attribution of flux partitioning variations between land surface models over the continental US. *Remote Sens.* 10, 751. <https://doi.org/10.3390/rs10050751>.
- Kurpius, M.R., Panek, J.A., Nikolov, N.T., McKay, M., Goldstein, A.H., 2003. Partitioning of water flux in a Sierra Nevada ponderosa pine plantation. *Agric. For. Meteorol.* 117 (3–4), 173–192. [https://doi.org/10.1016/S0168-1923\(03\)00062-5](https://doi.org/10.1016/S0168-1923(03)00062-5).
- Lauenroth, W.K., Bradford, J.B., 2006. Ecohydrology and the partitioning AET between transpiration and evaporation in a semiarid steppe. *Ecosystems.* 9, 756–767. <https://doi.org/10.1002/s10021-006-0063-8>.
- Lawrence, D.M., Oleson, K.W., Flanner, M.G., Thornton, P.E., 2011. Parameterization improvements and functional and structural advances in version 4 of the Community Land Model. *J. Adv. Model Earth Syst.* 3, M03001. <https://doi.org/10.1029/2011MS00045>.
- Lawrence, D.M., Thornton, P.E., Oleson, K.W., Bonan, G.B., 2007. The partitioning of evapotranspiration into transpiration, soil evaporation, and canopy evaporation in a GCM: impacts on land-atmosphere interaction. *J. Hydrometeorol.* 8 (4), 862–880. <https://doi.org/10.1175/jhm596.1>.
- Leuning, R., Cleugh, H.A., Zegelin, S.J., Hughes, D., 2005. Carbon and water fluxes over a temperate Eucalyptus forest and a tropical wet/dry savanna in Australia: measurements and comparison with MODIS remote sensing estimates. *Agric. For. Meteorol.* 129 (3–4), 151–173. <https://doi.org/10.1016/j.agrformet.2004.12.004>.
- Leuning, R., Zhang, Y.Q., Rajaud, A., Cleugh, H., Tu, K., 2008. A simple surface conductance model to estimate regional evaporation using MODIS leaf area index and the Penman-Monteith equation. *Water Resour. Res.* 44(10), 652–655. <https://doi:10.1029/2007WR006562>.
- Li, D., Pan, M., Cong, Z., Zhang, L., Wood, E., 2013. Vegetation control on water and energy balance within the Budkyo framework. *Water Resour. Res.* 49, 969–976. <https://doi.org/10.1029/wrcr.2010.7>.
- Lian, X., Piao, S., Huntingford, C., Li, Y., Zeng, Z., Wang, X., Ciais, P., McVicar, T.R., Peng, S., Ottlé, C., Yang, H., Yang, Y., Zhang, Y., Wang, T., 2018. Partitioning global land evapotranspiration using CMIP5 models constrained by observations. *Nature Clim. Change.* 8, 640–646. <https://doi.org/10.1038/s41558-018-0207-9>.
- Link, T., Unsworth, M., Marks, D., 2004. The dynamics of rainfall interception by a seasonal temperate rainforest. *Agric. For. Meteorol.* 124, 171–191. <https://doi.org/10.1016/j.agrformet.2004.01.010>.
- Liu, X.D., Li, Y.L., Chen, X.Z., Zhou, G.Y., Cheng, J., Zhang, D., Q., Meng, Z., Zhang, Q. M., 2015. Partitioning evapotranspiration in an intact forested watershed in southern China. *Ecohydrology.* 8 (6) <https://doi.org/10.1002/eco.1561>.
- Liu, Y., Liu, R., Chen, J.M., 2012. Retrospective retrieval of long-term consistent global leaf area index (1981–2011) from combined AVHRR and MODIS data. *Journal of Geophysical Research: Biogeosciences.* 117, G04003. <https://doi.org/10.1029/2012JG002084>.
- Liu, Y.Y., van Dijk, A.I.J.M., McCabe, M.F., Evans, J.P., de Jeu, R.A.M., 2013. Global vegetation biomass change (1988–2008) and attribution to environmental and human drivers: Global vegetation biomass change. *Global Ecol. Biogeogr.* 22 (6), 692–705. <https://doi.org/10.1111/geb.12024>.
- Loubet, B., Laville, P., Lehuger, S., Larmanou, E., Fléchard, C., Mascher, N., Génermont, S., Roche, R., Ferrara, R.M., Stella, P., Personne, E., Durand, B., Decuq, C., Flura, D., Masson, S., Fanucci, O., Rampon, J.N., Siemens, J., Kindler, R., Gabrielle, B., Schrumpf, M. and Cellier, P., 2011. Carbon, nitrogen and Greenhouse gases budgets over a four years crop rotation in northern France. *Plant Soil.* 343, 1/2, 109–137. <https://doi.org/10.1007/s11104-011-0751-9>.
- Ma, L.S., Li, Y.J., Wu, P.T., Zhao, X.N., Chen, X.L., Gao, X.D., 2020. Coupling evapotranspiration partitioning with water migration to identify the water consumption characteristics of wheat and maize in an intercropping system. *Agric. For. Meteorol.* 290 <https://doi.org/10.1016/j.agrformet.2020.108034>.
- Ma, S., Baldocchi, D.D., Xu, L., Hehn, T., 2007. Inter-Annual Variability In Carbon Dioxide Exchange Of An Oak/Grass Savanna And Open Grassland In California. *Agric. For. Meteorol.* 147 (3–4), 157–171. <https://doi.org/10.1016/j.agrformet.2007.07.008>.
- Ma, Y., Song, X.F., 2019. Applying stable isotopes to determine seasonal variability in evapotranspiration partitioning of winter wheat for optimizing agricultural management practices. *Sci Total Environ.* 654 (MAR.1), 633–642. <https://doi.org/10.1016/j.scitotenv.2018.11.176>.
- Marcolla, B., Cescatti, A., Manca, G., Zorer, R., Cavagna, M., Fiora, A., Gianelle, D., Rodeghiero, M., Sottocornola, M., Zampedri, R., 2011. Climatic controls and ecosystem responses drive the inter-annual variability of the net ecosystem exchange of an alpine meadow. *Agric. For. Meteorol.* 151 (9), 1233–1243. <https://doi.org/10.1016/j.agrformet.2011.04.015>.
- Maurer, E.P., Wood, A.W., Adam, J.C., Lettenmaier, D.P., Nijssen, B., 2002. A Long-Term Hydrologically Based Dataset of Land Surface Fluxes and States for the Conterminous United States. *J. Clim.* 15 (22), 3237. <https://doi.org/10.1175/JCLI-D-12-00508.1>.
- McCaughay, J., Pejam, M., Arain, M., Cameron, D., 2006. Carbon Dioxide And Energy Fluxes From A Boreal Mixedwood Forest Ecosystem In Ontario. Canada. *Agric. For. Meteorol.* 140 (1–4), 79–96. <https://doi.org/10.1016/j.agrformet.2006.08.010>.
- Merbold, L., Ardö, J., Arneth, A., Scholes, R.J., Nouvellon, Y., de Grandcourt, A., Archibald, S., Bonnefond, J.M., Boulain, N., Brueggemann, N., Brümmer, C., Cappelaere, B., Ceschia, E., El-Khidir, H.A.M., El-Tahir, B.A., Falk, U., Lloyd, J., Kerfoot, L., Dantec, V.L., Mougin, E., Muchinda, M., Mukelabai, M.M., Ramier, D., Rouspard, O., Timouk, F., Veenendaal, E.M., Kutsch, W.L., 2009. Precipitation as driver of carbon fluxes in 11 African ecosystems. *Biogeosciences.* 6 (6), 1027–1041. <https://doi.org/10.5194/bg-6-1027-2009>.
- Miralles, D.G., De Jeu, R.A.M., Gash, J.H., Holmes, T.R.H., Dolman, A.J., 2011. Magnitude and variability of land evaporation and its components at the global scale. *Hydro. Earth Syst. Sci.* 15, 967–981. <https://doi.org/10.5194/hess-15-967-2011>.
- Miralles, D.G., Gash, J.H., Holmes, T.R.H., De Jeu, R.A.M., Dolman, A.J., 2010. Global canopy interception from satellite observations. *J. Geophys. Res.-Atmos.* 115, D16122. <https://doi.org/10.1029/2009JD013530>.

- Miralles, D.G., Jiménez, C., Jung, M., Michel, D., Ershadi, A., McCabe, M.F., Hirschi, M., Martens, B., Dolman, A.J., Fisher, J.B., Mu, Q., Seneviratne, S.I., Wood, E.F., Fernández-Prieto, D., 2016. The WACMOS-ET project-Part 2: evaluation of global terrestrial evaporation data sets. *Hydrol. Earth Syst. Sci.* 20, 823–842. <https://doi.org/10.5194/hess-12-10651-2015>.
- Mitchell, P., Veneklaas, E., Lambers, H., Burgess, S., 2009. Partitioning of evapotranspiration in a semi-arid eucalypt woodland in south-western Australia. *Agric. For. Meteorol.* 149, 25–37. <https://doi.org/10.1016/j.agrformet.2020.108034>.
- Moureaux, C., Debacq, A., Bodson, B., Heinesch, B., Aubinet, M., 2006. Annual net ecosystem carbon exchange by a sugar beet crop. *Agric. For. Meteorol.* 139 (1–2), 25–39. <https://doi.org/10.1016/j.agrformet.2006.05.009>.
- Mu, Q.Z., Heinrichs, F.A., Zhao, M., Running, S.W., 2007. Development of a global evapotranspiration algorithm based on MODIS and global meteorology data. *Remote Sens. Environ.* 111, 519–536. <https://doi.org/10.1016/j.rse.2007.04.015>.
- Mu, Q.Z., Zhao, M., Running, S.W., 2011. Improvements to a MODIS global terrestrial evapotranspiration algorithm. *Remote Sens. Environ.* 115 (8), 1781–1800. <https://doi.org/10.1016/j.rse.2011.02.019>.
- Nemani, R.R., Keeling, C.D., Hashimoto, H., Jolly, W.M., Piper, S.C., Tucker, C.J., Myneni, R.B., Running, S.W., 2003. Climate-driven increases in global terrestrial net primary production from 1982 to 1999. *Science* 300, 1560–1563. <https://doi.org/10.1126/science.1082750>.
- Newman, B.D., Wilcox, B.P., Archer, S.R., Breshears, D.D., Dahm, C.N., Duffy, C.J., McDowell, N.G., Phillips, F.M., Scanlon, B.R., Vivoni, E.R., 2006. Ecohydrology of water-limited environments: A scientific vision. *Water Resour. Res.* 42, W06302. <https://doi.org/10.1029/2005WR004141>.
- Nizinski, J.J., Galat, G., Galat-Luong, A., 2011. Water balance and sustainability of eucalyptus plantations in the Kouilou basin (Congo-Brazzaville). *Russ. J. Ecol.* 42, 305–314. <https://doi.org/10.1134/S1067413611040126>.
- Noormets, A., McNulty, S.G., DeForest, J.L., Sun, G., Li, Q., Chen, J., 2008. Drought During Canopy Development Has Lasting Effect On Annual Carbon Balance In A Deciduous Temperate Forest. *New Phytol.* 179 (3), 818–828. <https://doi.org/10.1111/j.1469-8137.2008.02501.x>.
- Norman, J.M., Kustas, W.P., Humes, K.S., 1995. Source approach for estimating soil and vegetation energy fluxes in observations of directional radiometric surface-temperature. *Agric. For. Meteorol.* 77 (3–4), 263–293. [https://doi.org/10.1016/0168-1923\(95\)02265-Y](https://doi.org/10.1016/0168-1923(95)02265-Y).
- Oki, T., Kanae, S., 2006. Global Hydrological Cycles and World Water Resources. *Science* 313 (5790), 1068. <https://doi.org/10.1126/science.1128845>.
- Pan, M., Sahoo, A.K., Troy, T.J., Vinukollu, R.K., Sheffield, J., Wood, E.F., 2012. Multisource estimation of long-term terrestrial water budget for major global river basins. *J. Clim.* 25, 3191–3206. <https://doi.org/10.1175/JCLI-D-11-00300.1>.
- Prescher, A.K., Grünwald, T., Bernhofer, C., 2010. Land use regulates carbon budgets in eastern Germany: From NEE to NBP. *Agric. For. Meteorol.* 150, 1016–1025. <https://doi.org/10.1016/j.agrformet.2010.03.008>.
- Priestley, C.H.B., Taylor, R.J., 1972. On the assessment of surface heat flux and evaporation using large-scale parameters. *Mon. Weather Rev.* 100, 81–92. [https://doi.org/10.1175/1520-0493\(1972\)100<081:OTAOSH>2.3.CO;2](https://doi.org/10.1175/1520-0493(1972)100<081:OTAOSH>2.3.CO;2).
- Purdy, A.J., Fisher, J.B., Goulden, M.L., Colliander, A., Halverson, G., Tu, K., Famiglietti, J.S., 2018. SMAP soil moisture improves global evapotranspiration. *Remote Sens. Environ.* 219, 1–14. <https://doi.org/10.1016/j.rse.2018.09.023>.
- Pypker, T.G., Bond, B.J., Link, T.E., Marks, D., Unsworth, M.H., 2005. The importance of canopy structure in controlling the interception loss of rainfall: examples from a young and an old-growth Douglas-fir forest. *Agric. For. Meteorol.* 130, 113–129. <https://doi.org/10.1016/J.AGRFORMAT.2005.03.003>.
- Rambal, S., Joffre, R., Ourcival, J.M., Cavender-Bares, J., Rocheteau, A., 2004. The growth respiration component in eddy CO<sub>2</sub> flux from a *Quercus ilex* mediterranean forest. *Glob. Chang. Biol.* 10 (9), 1460–1469. <https://doi.org/10.1111/j.1365-2486.2004.00819.x>.
- Raz-Yaseef, N., Billesbach, D.P., Fischer, M.L., Biraud, S.C., Gunter, S.A., Bradford, J.A., Torn, M.S., 2015. Vulnerability Of Crops And Native Grasses To Summer Drying In The U.S. Southern Great Plains. *Agriculture, Ecosystems & Environment* 213, 209–228. <https://doi.org/10.1016/j.agee.2015.07.021>.
- Raz-Yaseef, N., Yakir, D., Schiller, G., Cohen, S., 2012. Dynamics of evapotranspiration partitioning in a semi-arid forest as affected by temporal rainfall patterns. *Agric. For. Meteorol.* 157, 77–85. <https://doi.org/10.1016/j.agrformet.2012.01.015>.
- Rothstein, D.E., Zak, D.R., Pregetz, K.S., Curtis, P.S., 2000. Kinetics Of Nitrogen Uptake By *Populus tremuloides* In Relation To Atmospheric CO<sub>2</sub> And Soil Nitrogen Availability. *Tree Physiol.* 20 (4), 265–270. <https://doi.org/10.1093/treephys/20.4.265>.
- Rousseaux, M.C., Figuerola, P.I., Correa-Tedesco, G., Searles, P.S., 2009. Seasonal variations in sap flow and soil evaporation in an olive (*Olea europaea* L.) grove under two irrigation regimes in an arid region of Argentina. *Agric. Water Manage.* 96 (6), 1037–1044. <https://doi.org/10.1016/j.agwat.2009.02.003>.
- Ruehr, N.K., Martin, J.G., Law, B.E., 2012. Effects Of Water Availability On Carbon And Water Exchange In A Young Ponderosa Pine Forest: Above- And Belowground Responses. *Agric. For. Meteorol.* 164, 136–148. <https://doi.org/10.1016/j.agrformet.2012.05.015>.
- Saleska, S. R., Miller, S. D., Matross, D. M., Goulsen, M. L., Wofsy, S. C., Rocha, H. R. da, Camargo, P. B. de, Crill, P., Daube, B. C., Freitas, H. C. de, Hutyra, L., Keller, M., Kirchhoff, V., Menton, M., Munger, J. W., Pyle, E. H., Rice, A. H., Silva, H., 2003. Carbon In Amazon Forests: Unexpected Seasonal Fluxes And Disturbance-Induced Losses. *Science* 302(5650), 1554–1557. <https://doi.org/10.1126/science.1091165>.
- Schlésinger, W. H., Jasechko, S., 2104. Transpiration in the global water cycle. *Agric. For. Meteorol.* 189–190, 115–117. <https://doi.org/10.1016/j.agrformet.2014.01.011>.
- Scott, R.L., Huxman, T.E., Cable, W.L., Emmerich, W.E., 2006. Partitioning of evapotranspiration and its relation to carbon dioxide exchange in a Chihuahuan Desert shrubland. *Hydro. Processes.* 20, 3227–3243. <https://doi.org/10.1002/hyp.6329>.
- Scott, R.L., Biederman, J.A., Hamerlynck, E.P., Barron-Gafford, G., 2015. The carbon balance pivot point of southwestern U.S. semiarid ecosystems: Insights from the 21st century drought. *J. Geophys. Res. Biogeosci.* 120, 2612–2624. <https://doi.org/10.1002/2015JG003181>.
- Shuttleworth, W.J., 1988. Evaporation from Amazonian rainforest. *Proc. Roy. Soc. London.* 233B, 321–346. <https://doi.org/10.1098/rspb.1988.0024>.
- Smith, S.D., Herr, C.A., Leary, K.L., Piorkowski, J.M., 1995. Soil-plant water relations in a Mojave Desert mixed shrubcommunity: a comparison of three geomorphic surfaces. *J. Arid Environ.* 29, 339–351. [https://doi.org/10.1016/S0140-1963\(05\)80113-2](https://doi.org/10.1016/S0140-1963(05)80113-2).
- Song, L.N., Zhu, J.J., Li, M.C., Zhang, J.X., Zheng, X., Wang, K., 2018. Canopy transpiration of *Pinus sylvestris* var. *mongolica* in a sparse wood grassland in the semiarid sandy region of Northeast China. *Agric. For. Meteorol.* 250, 192–201. <https://doi.org/10.1016/j.jenvman.2021.112306>.
- Soubie, R., Heinesch, B., Granier, A., Aubinet, M., Vincke, C., 2016. Evapotranspiration assessment of a mixed temperate forest by four methods: Eddy covariance, soil water budget, analytical and model. *Agric. For. Meteorol.* 228–229, 191–204. <https://doi.org/10.1016/j.agrformet.2016.07.001>.
- Stoy, P.C., Katul, G.G., Siqueira, M.B.S., Juang, J., Novick, K.A., McCarthy, H.R., Oishi, A. C., Uebelherr, J.M., Kim, H.S., Oren, R., 2006. Separating the effects of climate and vegetation on evapotranspiration along a successional chronosequence in the southeastern U.S. *Glob. Chang. Biol.* 12, 2115–2135. <https://doi.org/10.1111/j.1365-2486.2006.01244.x>.
- Sun, X., Wilcox, B.P., Zou, C.B., 2019. Evapotranspiration partitioning in dryland ecosystems: a global meta-analysis of in situ studies. *J. Hydrol.* 576, 123–136. <https://doi.org/10.1016/j.jhydrol.2019.06.022>.
- Suni, T., Rinne, J., Reissell, A., Altimir, N., Keronen, P., Rannik, Ü., Maso, M.D., Kulmala, M., Vesala, T., 2003. Long-term measurements of surface fluxes above a Scots pine forest in Hyttälä, southern Finland, 1996–2001. *Boreal Env. Res.* 8, 287–301.
- Suyker, A., Verma, S., Burba, G., Arkebauer, T., Walters, D., Hubbard, K., 2004. Growing Season Carbon Dioxide Exchange In Irrigated And Rainfed Maize. *Agric. For. Meteorol.* 124 (1–2), 1–13. <https://doi.org/10.1016/j.agrformet.2004.01.011>.
- Talsma, C.J., Good, S.P., CaRlos, J., Martens, B., Fisher, J.B., Miralles, D.G., McCabe, M. F., Purdy, A.J., 2018. Partitioning of evapotranspiration in remote sensing-based models. *Agric. For. Meteorol.* 260–261, 131–143. <https://doi.org/10.1016/j.agrformet.2018.05.010>.
- Tang, J., Bolstad, P.V., Ewers, B.E., Desai, A.R., Davis, K.J., Carey, E.V., 2006. Sap flux-upscaled canopy transpiration, stomatal conductance, and water use efficiency in an old growth forest in the Great Lakes region of the United States. *J. Geophys. Res. Biogeosci.* 111 (G02009) <https://doi.org/10.1029/2005JG000083>.
- Thomas, F., Christina, B., Narasinha, S.J., 2016. FLUXNET2015 RU-Vrk Seida/Vorkuta. N. P., Russian Federation <https://doi.org/10.18140/FLX/1440245>.
- Trenberth, K.E., Falutti, J.T., Kiehl, J., 2009. Earth's global energy budget. *Bull Am Meteorol Soc.* 90, 311–323. <https://doi.org/10.1175/2008BAMS2634.1>.
- Unsworth, M.H., Phillips, N., Link, T., Bond, B., Falk, M., Harmon, M., Hinckley, T., Marks, D., Paw, U.K.-T., 2004. Components and Controls of Water Flux in an Old-growth Douglas-fir-Western Hemlock Ecosystem. *Ecosystems*. 7, 468–481. <https://doi.org/10.1007/s10021-004-0138-3>.
- Valente, F., David, J.S., Gash, J.H., 1997. Modelling interception loss for two sparse eucalypt and pine forests in central Portugal using reformulated Rutter and Gash analytical models. *J. Hydrol.* 190, 141–162. [https://doi.org/10.1016/S0022-1694\(96\)03066-1](https://doi.org/10.1016/S0022-1694(96)03066-1).
- Valentini, R., De Angelis, P., Matteucci, G., Monaco, R., Dore, S., Mugnocco, G.E.S., 1996. Seasonal net carbon dioxide exchange of a beech forest with the atmosphere. *Glob. Chang. Biol.* 2 (3), 199–207. <https://doi.org/10.1111/j.1365-2486.1996.tb0072.x>.
- Vickers, D., Thomas, C., Law, B.E., 2009. Random And Systematic CO<sub>2</sub> Flux Sampling Errors For Tower Measurements Over Forests In The Convective Boundary Layer. *Agric. For. Meteorol.* 149 (1), 73–83. <https://doi.org/10.1016/j.agrformet.2008.07.005>.
- Vinukollu, R.K., Meynadier, R., Sheffield, J., Wood, E.F., 2011a. Multi-model, multi-sensor estimates of global evapotranspiration: climatology, uncertainties and trends. *Hydro. Processes.* 25 (26), 3993–4010. <https://doi.org/10.1002/hyp.8393>.
- Vinukollu, R. K., Wood, E. F., Ferguson, C. R., Fisher, B., 2011b. Global Estimates of evapotranspiration for Climate Studies using Multi-Sensor Remote Sensing Data: evaluation of Three Process-Based Approaches. *Remote Sens. Environ.* 115(3). <https://doi.org/10.1016/j.rse.2010.11.006>.
- Wang, C., Bond-Lamberty, B., Gower, S.T., 2003. Carbon Distribution Of A Well- And Poorly-Drained Black Spruce Fire Chronosequence. *Glob. Chang. Biol.* 9 (7), 1066–1079. <https://doi.org/10.1046/j.1365-2486.2003.00645.x>.
- Wang, D., Wang, L., 2017. Dynamics of evapotranspiration partitioning for apple trees of different ages in a semiarid region of northwest China. *Agric. Water Manage.* 191, 1–15. <https://doi.org/10.1016/j.agwat.2017.05.010>.
- Wang, K., Dickinson, R.E., 2012. A review of global terrestrial evapotranspiration: Observation, modeling, climatology, and climatic variability. *Rev. Geophys.* 50, RG2005. <https://doi.org/10.1029/2011RG000373>.
- Wang, L., Good, S.P., Taylor, K.K., 2014. Global synthesis of vegetation control on evapotranspiration partitioning. *Geophys. Res. Lett.* 41, 6753–6757. <https://doi.org/10.1002/2014GL061439>.
- Wang, S., Pan, M., Mu, Q., Shi, X., Mao, J., Brümmer, C., Jassal, R.S., Krishnan, P., Li, J., Black, T.A., 2015. Comparing Evapotranspiration from Eddy Covariance Measurements, Water Budgets, Remote Sensing, and Land Surface Models over agrformet.2014.01.011.

- Canada. J. Hydrometeorol. 16, 1540–1560. <https://doi.org/10.1175/JHM-D-14-0189.1>.
- Wang-Erlundsson, L., van der Ent, R. J., Gordon, L. J., Savenije, H. H. G., 2014. Contrasting roles of interception and transpiration in the hydrological cycle – Part 1: Temporal characteristics over land. Earth Syst. Dynam. 5, 441–469. <https://doi.org/10.5194/esd-5-441-2014>, 2014.
- Wei, Z., Yoshimura, K., Wang, L., Miralles, D.G., Jasechko, S., Lee, X., 2017. Revisiting the contribution of transpiration to global terrestrial evapotranspiration. Geophys. Res. Lett. 44, 2792–2801. <https://doi.org/10.1002/2016GL072235>.
- Wilson, K.B., Hanson, P.J., Mulholland, P.J., Baldocchi, D.D., Wullschleger, S.D., 2001. A comparison of methods for determining forest evapotranspiration and its components: sap-flow, soil water budget, eddy covariance and catchment water balance. Agric. For. Meteorol. 106 (2), 153–168. [https://doi.org/10.1016/S0168-1923\(00\)00199-4](https://doi.org/10.1016/S0168-1923(00)00199-4).
- Wohlfahrt, G., Hammerle, A., Haslwanter, A., Bahn, M., Tappeiner, U., Cernusca, A., 2008. Seasonal and inter-annual variability of the net ecosystem CO<sub>2</sub> exchange of a temperate mountain grassland: Effects of weather and management. J. Geophys. Res. 113 (D8), D08110. <https://doi.org/10.1029/2007JD009286>.
- Woodhouse, I.H., 2005. Introduction to Microwave Remote Sensing. CRC Press.
- Xu, Z.W., Zhu, Z.L., Liu, S.M., Song, L.S., Wang, X.C., Zhou, S., Yang, X.F., Xu, T.R., 2021. Evapotranspiration partitioning for multiple ecosystems within a dryland watershed: Seasonal variations and controlling factors. J. Hydrol. 598 <https://doi.org/10.1016/j.jhydrol.2021.126483>.
- Yan, H., Yu, Q., Zhu, Z.C., Myneni, R.B., Yan, H.M., Wang, S.Q., Shugart, H.H., 2013. Diagnostic analysis of interannual variation of global land evapotranspiration over 1982–2011: Assessing the impact of ENSO. J. Geophys. Res. Atmos. 118 (16), 8969–8983. <https://doi.org/10.1002/jgrd.50693>.
- Yu, G.R., Wen, X.F., Sun, X.M., Tanner, B.D., Lee, X.H., Chen, J.Y., 2006. Overview of ChinaFLUX and evaluation of ist eddy covariance measurement. Agric. For. Meteorol. 137, 125–137. <https://doi.org/10.1016/j.agrformet.2006.02.011>.
- Zhang, K., Kimball, J. S., Nemani, R. R., Running, S. W., 2010. A continuous satellite-derived global record of land surface evapotranspiration from 1983 to 2006. Water Resour. Res. 46: W09522. <https://doi.org/10.1029/2009WR008800>.
- Zhang, Y.Q., Pena-Arancibia, J.L., McVicar, T.R., Chiew, F.H.S., Vaze, J., Liu, C.M., Lu, X.J., Zheng, H.X., Wang, Y.P., Liu, Y.Y., Miralles, D.G., Pan, M., 2016. Multi-decadal trends in global terrestrial evapotranspiration and its components. Sci Rep-Uk. 6, 19124. <https://doi.org/10.1038/srep19124>.
- Zheng, C., Jia, L., 2020. Global canopy rainfall interception loss derived from satellite earth observations. Ecohydrology. 13, 1–13. <https://doi.org/10.1002/eco.2186>.
- Zheng, J., Fan, J.L., Zhang, F.C., Zhuang, Q.L., 2021. Evapotranspiration partitioning and water productivity of rainfed maize under contrasting mulching conditions in Northwest China. Agric. Water Manage. 243 <https://doi.org/10.1016/j.agwat.2020.106473>.
- Zhou, G.Y., Yin, G.C., Morris, J., Bai, J.Y., Chen, S.X., Chu, G.W., Zhang, N.N., 2004. Measured Sap Flow and Estimated Evapotranspiration of Tropical Eucalyptus urophylla Plantations in South China. Acta Botanica Sinica. 46 (2) <https://doi.org/10.1614/WS-03-091R>.
- Zhou, S., Yu, B., Zhang, Y., Huang, Y., Wang, G., 2016. Partitioning evapotranspiration based on the concept of underlying water use efficiency. Water Resour. Res. 52 <https://doi.org/10.1002/2015WR017766>.
- Zhu, G.F., Zhang, K., Chen, H.L., Wang, Y.Q., Sun, Y.H., Zhang, Y., Ma, J.Z., 2019. Development and evaluation of a simple hydrologically based model for terrestrial evapotranspiration simulations. J. Hydrol. 577 <https://doi.org/10.1016/j.jhydrol.2019.123>.
- Zielis, S., Etzold, S., Zweifel, R., Eugster, W., Haeni, M., Buchmann, N., 2014. NEP of a Swiss subalpine forest is significantly driven not only by current but also by previous year's weather. Biogeosciences. 11 (6), 1627–1635. <https://doi.org/10.5194/bg-11-1627-2014>.